Detecting Disease in Citrus Trees using Multispectral UAV Data and Deep Learning Algorithm

A research report submitted to the Faculty of Science, University of the Witwatersrand, Johannesburg, in partial fulfilment of the requirements for the degree of Master of Science (Geographical Information Systems and Remote Sensing) at the School of Geography, Archaeology & Environmental Studies

Logan Woolfson
(1055822)

Supervisor:
Dr. Elhadi Adam

20th June 2024

Candidate's Declaration

I declare that this research report is my own, unaided work. It is being submitted for the Degree of Master of Science at the University of the Witwatersrand, Johannesburg. It has not been submitted before for any degree or examination at any other University.

(Signature of candidate)

20th day of June 2024, at Johannesburg.

Abstract

There is a high prevalence, in South Africa, of fruit tree related diseases infesting lemon trees, subsequently affecting overall crop yield and quality. Ultimately, the income for the farmers is significantly diminished and limits the supply of nutritional food crops for the South African population, who already suffer from a high incidence of malnutrition. Currently, there are various methods utilized to detect diseases in fruit trees, however they pose limitations in terms of efficiency and accuracy. By employing the use of drones and machine learning methods, fruit tree diseases could be detected at an earlier stage of development and with a much higher level of accuracy. Consequently, the chances of remedying the trees before the disease spreads is greatly improved, and the supply of nutritious fruit within South Africa is increased.

This research report's aim is to investigate the effectiveness of a deep learning algorithm for detecting and classifying diseases in lemon orchards using multispectral drone imagery. This entails assessing the performance of a pretrained ResNet-101 model, fine-tuned with additional sample images, in accurately identifying and classifying diseased lemon trees, specifically those affected by Phytophthora root rot. The methodology involves the utilization of a pretrained ResNet-101 model, a deep learning architecture, and the retraining of its layers with an augmented dataset from multispectral aerial drone images of a lemon orchard. The model is fine-tuned to enhance its ability to discern subtle spectral variations indicative of disease presence. The selection of ResNet-101 is grounded in its proven success in image recognition tasks and transfer learning capabilities.

The results obtained demonstrated an impressive accuracy of 80%. The deep learning algorithm exhibited notable performance in distinguishing root rot-affected lemon trees from their healthy counterparts. The findings indicate the promise of utilizing advanced deep learning methods for timely and effective disease detection in agricultural farmlands, facilitating orchard management.

Keywords: Citrus Disease, Deep Learning, Multispectral UAV, Resnet-101, Phytophthora Root Rot

Acknowledgements

I extend my appreciation to all members of the team at El Sundew farm for their support and generosity during my Masters research. The opportunity to collect data on their lemon trees has been invaluable to the success of my project. The kindness and cooperation extended by the team made the entire research process seamless and enjoyable. Their willingness to share their expertise and resources, significantly contributed to the depth and quality of my study. I am thankful for the assistance provided by Stephan, Lehan and LJ.

I would like to express gratitude to my supervisor, Dr. Elhadi Adam, for providing invaluable feedback and guidance throughout the research process. I would also like to acknowledge Dr. Philemon Tsele for his pivotal role in facilitating UAV data acquisition and pre-processing. His dedicated time and effort are truly appreciated.

A big thank you is also given to my long-time friend Jared for your invaluable assistance with the ground truth data collection. Your dedication and attention to detail greatly contributed to the success of the project, and I truly appreciate the time and effort you put in. Collaborating with a good friend like you not only made the research process more enjoyable but also enhanced its outcomes. Thank you once again for your unwavering support and friendship.

Table of Contents

List of Figures

List of Tables

Chapter 1: Introduction

1.1. General Introduction

Crop diseases pose a significant threat to agricultural productivity, resulting in yield and economic losses for farmers (Ristaino *et al.*, 2021). Lemons are a popular crop in South Africa with an estimated production of 625 000 tons in 2021 (USDA, 2021). The value of lemon exports exceeded R6.1 billion per annum in 2021, making up approximately 10% of the global lemon exports (ITC, 2021). Despite the relative economic significance of lemon production in South Africa, lemon trees face numerous pest and disease stresses, such as Phytophthora root rot.

Phytophthora root rot, caused by various *Phytophthora spp.,* has emerged as a prevalent threat to citrus orchards globally, posing a significant risk to lemon trees (Citrus limon). Originating from the soil, this pathogen causes severe damage to the roots of susceptible plants, compromising their ability to absorb water and nutrients (Maseko and Coutinho, 2002). This is a common lemon tree disease in Limpopo, a regional boundary within South Africa. Trees infected with Phytophthora initially show signs such as small leaves, sparse foliage, and stunted growth. Infected trees can deteriorate over several years or rapidly within the same growing season. Phytophthora pathogens can remain in the soil for extended periods, becoming active during periods of moisture and moderate temperatures. (Wiesman, 2009).

Conventional techniques like visual inspection and manual sampling for identifying crop diseases are often laborious and time-intensive, posing challenges for large-scale monitoring (Latif, 2019). Nonetheless, recent progress in remote sensing, notably the utilization of multispectral drone imagery, has demonstrated significant results in the early detection and forecasting of crop diseases (Li *et al.*, 2022). These drone images offer high-resolution and multi-temporal data, capable of capturing nuanced variations in plant health, thereby enabling precise and timely disease detection (Maimaitijiang *et al.*, 2020). The integration of Unmanned Aerial Vehicle (UAV) remote sensing approaches with deep learning techniques presents an innovative solution (Musci *et al.*, 2020). UAVs equipped with remote sensing technologies offer a high spatial and spectral resolution capability that can significantly enhance the speed and efficiency of disease detection in large orchards (Jay *et al.*, 2019). The advantages of using UAVs in conjunction with deep learning methodologies, such as ResNet-101, lie in their ability to extract significant features (Shahi *et al.*, 2023).

Typical techniques employed in remote sensing to monitor crop diseases include: vegetation indices and machine learning to classify diseased fruit trees. Hyperspectral imaging sensors mounted on a UAV can accurately detect citrus canker disease using vegetation indices. One example is the Modified Chlorophyll Absorption in Reflectance Index (Abdulridha *et al.*, 2019). Citrus canker and Phytophthora root rot are both diseases that affect citrus trees and can lead to significant economic losses for citrus growers. Despite affecting different parts of the tree and being caused by different pathogens (bacteria for citrus canker and Phytophthora fungi for root rot), they share the similar symptoms. While the symptoms may manifest differently due to the nature of the pathogens involved, both diseases can cause visible signs of distress in citrus trees. These symptoms may include leaf yellowing, defoliation, twig dieback, and overall decline in tree health (Bock *et al.*, 2009). The research by Abdulridha et al.

(2019) demonstrated that machine learning algorithms such as radial basis function (RBF) and K nearest neighbour (KNN) can achieve over 90% classification accuracy for identifying canker infected fruit trees, when using hyperspectral UAV based imagery (Abdulridha *et al.*, 2019). A similar machine learning approach has been used by Dadras Javan *et al.* (2019), where multispectral images was used to detect greening disease in citrus trees. Five bands were captured; red, green, blue, red-edge and near-infrared (NIR). Sixteen vegetation indices were generated and fed into a support vector machine (SVM) model to classify the UAV images. This was done in two steps; the first classified trees from non-tree objects and the second classified healthy and diseased trees. The overall classification accuracy was 81.75% for the SVM model (Dadras Javan *et al.*, 2019).

Deep learning, a subset of machine learning has also become a popular option when selecting a model for a UAV based dataset. A study by Osco *et al.* (2021) demonstrated the efficacy of several pixelwise methods such as fully convolutional network and U-Net to accurately segment citrus orchards using a multispectral UAV dataset. An F1 score of 94% was achieved in this study, which shows impressive results for deep learning methods (Osco *et al.*, 2021).

There is a large need for monitoring and detecting diseases within lemon orchards in South Africa due to the large farmland dedicated to growing this crop. The earlier the disease is picked up, the sooner treatment can be applied. Phytophthora root rot is a common lemon tree disease in Limpopo, a regional boundary within South Africa (Meitz-Hopkins *et al.*, 2014). This early intervention can mitigate against the further spread and damage to the tree and thereby reducing losses in yield, ultimately boosting revenue for the farmer (Peng *et al.*, 2022). Furthermore, understanding the spatial distribution of the detected disease aids farmers in making informed economic decisions regarding the implementation of disease management strategies (Meitz-Hopkins *et al.*, 2014).

This research attempts to leverage the advantages of UAV remote sensing coupled with deep learning to investigate the performance of the ResNet-101 model to accurately identify Phytophthora root rot in a lemon orchard. Doing so contributes to the advancement of precision agriculture but also to the sustainable management of citrus orchards by minimizing the impact of this devastating pathogen.

1.2. Problem Statement

Citrus tree root rot, a serious Phytophthora disease, poses a significant challenge in key citrus-producing provinces in South Africa, including Limpopo, Mpumalanga, and Western and Eastern Cape (Van Der Merwe, 2020). The prevalence of Phytophthora root rot in Limpopo is a major concern, though specific statistics for South Africa are not available. A survey in Texas, USA, showed root rot symptoms in 33.7% of trees across 37 orchards (Chaudhary *et al.*, 2020).

Phytophthora species have a destructive impact on citrus production, particularly affecting lemon trees by damaging the root system and causing a decline in health and productivity (Meitz-Hopkins *et al.*, 2014; Anas Fadli *et al.*, 2022). Symptoms include yellowing leaves, leaf drop, and feeder root destruction, leading to stunted growth and reduced yields (Pest Management Guidelines, 2019). Current detection methods are labour-intensive, time-consuming, and prone to human error (Field Diagnosis and Management of Phytophthora Diseases, 2018), demanding improved monitoring systems. A field-based detection method by Gaikwad *et al.* (2023) showed promise but was limited to small orchards. Remote sensing, particularly multispectral UAV imaging, offers advantages such as rapid area analysis and tracking temporal changes. Deep learning approaches can extract intricate features from UAV images for precise insights (Marcato Junior *et al.*, 2021). However, these methods require substantial processing power (Wang *et al.*, 2019).

Farmers need high spatial and temporal resolution data to manage disease outbreaks. While satellite remote sensing provides high temporal resolution, it lacks the spatial resolution of UAVs (Dube and Mutanga, 2015; Li *et al.*, 2015). UAVs offer near real-time data acquisition, high accuracy, and affordability, making them ideal for detailed disease detection (Yue *et al.*, 2012; Garza *et al.*, 2020; Trajkovski *et al.*, 2020). Existing deep learning models like U-net and Resnet have been used for disease detection in various crops (Shahi *et al.*, 2023; Kouadio *et al.*, 2023), but research on detecting Phytophthora root rot in lemon trees in Limpopo using multispectral UAVs is limited.
Addressing these gaps can advance remote sensing in agriculture, enabling effective disease prediction and management, leading to healthier crops and increased yields.

1.3. The Aim of the Study

The main research aim is to detect disease in citrus trees using multispectral UAV data and deep learning algorithm.

This was achieved through the research objectives:

I. Determine if there is a statistical significant difference in the average pixel value between healthy and diseased lemon trees, across each reflectance band captured by the UAV sensor using the appropriate f-tests and t-tests.
II. Examine the effectiveness of the ResNet-101 deep learning model in accurately predicting the disease status of lemon trees based on multispectral data.
III. Investigate the spatial distribution of the diseased lemon trees.

1.4. Research Report Outline

This report is comprised of five main chapters. The **first chapter** gives a brief introduction, offering an overview of the study, its objectives, problem statement, and aim of the report. In the **second chapter**, a literature review is presented, which explores previous research pertinent to the study. This section also explores scientific literature on Phytophthora root rot within South Africa, as well as how fruit tree diseases are mapped globally. In the **third chapter**, a comprehensive description of the techniques and methods employed to achieve the specific objectives is provided. This includes an overview of the study area, and insights into data collection, processing, and analysis. The **fourth chapter** presents the primary findings derived from the study, while the **fifth chapter** engages in a discussion which compares the results for these findings, to existing research. Lastly, the **sixth chapter** provides the main findings, acknowledges existing limitations, and offers recommendations for similar research endeavours.

Chapter 2: Literature Review

2.1. Background of Phytophthora Root Rot

Phytophthora root rot is a devastating disease that affects a wide range of trees, caused by various Phytophthora species. This disease is particularly destructive as it can lead to the death of infected trees by spreading through the roots (Meitz-Hopkins *et al.*, 2014). Erwin and Ribeiro's (1996) comprehensive work also provides insights into the biology and management of Phytophthora diseases, forming a foundational understanding of the challenges faced by citrus growers. The three common species of Phytophthora are *P. infestons, P. cinnamomi, and P. palmivora* have originated in different locations. *P. infestons* have originated from Mexico, *P. cinnamomi* is thought to have originated from New Guinea, Indonesia and South Africa. *P. palmivora* has a possible origin from South America (Zentmyer, 1988). Phytophthora root rot thrives in wet and poorly drained soil conditions, making it a significant threat to various plant and tree species. The disease is primarily caused by soil-borne microorganisms known as Phytophthora species (Savita and Nagpal, 2012). These pathogens produce spores that can move through water, infecting fine roots initially and progressing to larger roots, and the stem of the plant under favourable conditions (Graham, 2013).

2.2. Phytophthora Root Rot Symptoms

Initial symptoms of Phytophthora root rot include wilting, yellowing and sparse foliage. In trees, foliage may change from vibrant green to brown (Ramírez-Gil *et al.*, 2017). Signs of Phytophthora root rot encompass root necrosis, stunted growth, and persistent wilting (Mestas, 2018). Examination below the surface may reveal a poor root system with rotted fine feeder roots and decayed larger roots. The internal roots may appear black or brown, indicating infection by Phytophthora (Salgadoe *et al.*, 2018). Distinguishing the disease from flooding damage or nematodes can be challenging, often needing laboratory analysis for accurate identification. (Joubert and Labuschagne, 1998). In the later stages of infection, the rate of root death surpasses the production of new roots. Consequently, the tree struggles to sustain sufficient water and mineral uptake, as well as nutrient stores, which are depleted due to repeated severe fungal attacks (Savita and Nagpal, 2012). As a consequence, fruit size and production diminish, accompanied by leaf loss and twig dieback within the canopy (Savita and Nagpal, 2012).

2.3. Factors Influencing Phytophthora Root Rot Spread

Phytophthora root rot, caused by various *Phytophthora spp*., is influenced by multiple factors that impact the virulence and spread of the pathogen within trees. The duration of soil saturation is a factor which significantly influences the development and spread of Phytophthora root rot. Excessive soil moisture, paired with temperatures between 25 °C – 30 °C, creates favourable conditions for disease progression (Giachero *et al.*, 2022).

A review by Savita and Nagpal (2012), highlight the following ways in which *Phytophthora spp*. are spread. The main way *Phytophthora spp.* spread in citrus orchards is through infected nursery plants. Alternatively, these species spread through various means: roots in the soil, surface water, splashing water from the ground onto the plant, and through the air from infected parts of the plant. Variations in pathogen strain and species can impact the severity and spread of Phytophthora root rot. Understanding the genetic traits of the pathogen is crucial for effective disease management strategies (Barchenger *et al.*, 2023).

Savita and Nagpal (2012) also mentions that even if there are no signs of disease, the pathogen can still be in the soil or roots. It can also be carried in the soil on equipment like vehicles moving from infected to non-infected areas. When the soil dries, the number of pathogens goes down, which makes spreading less likely. Irrigation water can also move the pathogen around, especially in places that use furrow or flood irrigation (Savita and Nagpal, 2012). Rainwater can carry the fungus away from the orchard when it drains. In places with irrigated citrus, problems can be worse when water runoff carries the pathogen into canals or ponds, which then spreads to other areas. Wind isn't a big factor in spreading *Phytophthora spp.*, but soil blown by the wind can carry contaminated soil in areas that was free of the pathogen (Savita and Nagpal, 2012). Rain carried by the wind can also spread spores produced on the surface of the plant. Different environmental factors, like weather, also affect how diseases develop, the severity and how the pathogen spreads and survives (Savita and Nagpal, 2012).

Implementing preventative farming measures like avoiding planting in previously affected areas, maintaining proper soil drainage and avoiding over watering the base of trees through automated irrigation systems can help manage Phytophthora root rot (Giachero *et al.*, 2022). Soil factors, such as compaction caused by the use of heavy farming equipment, can affect tree growth and root development, increasing the likelihood of Phytophthora root rot (Joubert and Labuschagne, 1998). Abiotic stressors, like root asphyxiation, mineral disorders, and phytotoxicity, can further impact the health of roots and further progress Phytophthora root rot (Swart, 2018). The presence of insect pests like citrus root weevil can exacerbate the disease by wounding the roots, providing entry points for the pathogen (Swart, 2018). The application of fungicides can aid in controlling Phytophthora diseases in plants. Preventive fungicide sprays have shown high efficacy in managing Phytophthora rot (Chaudhary *et al.*, 2020). Management strategies for Phytophthora root rot in citrus trees also include irrigation management, and by using resistant rootstocks (Joubert and Labuschagne, 1998).

2.4. Phytophthora Root Rot Impacts in South Africa

Phytophthora root rot has a significant impact on citrus trees in South Africa, causing severe damage and affecting the overall health of the trees. The disease is particularly severe in South Africa due to the high soil temperatures and excessive moisture received via summer rainfall, which favours the growth and spread of Phytophthora species (Nagle *et al.*, 2013). Africans rely on agriculture, therefore plant diseases could interfere with the livelihood of a large number of the population and commercial business who grow and export crops as a source of income. Late disease detection cause by Phytophthora may result in total loss of the crop or orchard (Nagle *et al.*, 2013). In South Africa, it is estimated that 10% of the annual gross value of avocados is lost due to root rot caused by *P. cinnamomi* (Nagle *et al.*, 2013).

Phytophthora significantly impacts the socio-economic landscape of African countries and their inhabitants, particularly South Africa and its province Limpopo. Notably, agricultural losses due to pathogens like *P. infestans* have a profound effect on potato and tomato yields (Abdulridha *et al.*, 2020). The devastating impact of Black pod disease on cacao production, particularly in Africa, the largest producer, further exacerbates economic challenges. This disease directly affects resource-poor farmers who rely on cacao as a primary source of income. Additionally, avocado production faces severe setbacks due to *P. cinnamomi*, resulting in substantial economic losses for farmers (Nagle *et al.*, 2013).

2.5. Mapping Disease in Fruit Trees

2.5.1. Multispectral and Hyperspectral Data

The integration of UAV-based remote sensing provides high-resolution spatial and spectral data that is important in disease detection. Sankaran et al. (2015) emphasizes the potential of UAVs in monitoring plant health, and the focus on multispectral data by Mahlein (2016) highlights its significance in capturing subtle physiological changes in plants. The data and insight offered by multispectral UAV data beyond the visible spectrum becomes particularly relevant for the analysis of plant health. The additional spectral information allows for a more complex analysis of citrus tree health, enabling the early identification of Phytophthora root rot.

A novel remote sensing technique was developed by Abdulridha *et al.* (2019) to identify citrus canker under laboratory conditions and subsequently validated in the field using a UAV. In the lab, a hyperspectral imaging system, which covers wavelengths from 400 to 1000 nm, was used to spot citrus canker at three different stages of the disease on Sugar Belle leaves and young fruit. To do this, two methods were used to classify the data namely RBF and KNN. The same imaging system, when mounted on a UAV, was also used to spot citrus canker on tree canopies in the orchard. The results showed that the RBF method had better overall accuracy in classifying canker presence in leaves at the three disease stages (94%, 96%, and 100%) compared to the KNN method (94%, 95%, and 96%) (Abdulridha *et al.*, 2019).

Moriya *et al.* (2021) utilized hyperspectral remote sensing images taken by UAVs to detect citrus gummosis disease caused by the fungus *Phytophthora spp.,* demonstrating effective disease mapping capabilities. The classification maps were produced by training a supervised machine learning algorithm called Spectral Angle Mapper (SAM) to indicate the health status of citrus plants. The model achieved an accuracy of 79% using multispectral data and 94% using all 25 bands of the hyperspectral sensor (Moriya *et al.*, 2021).

Moreover, Fletcher *et al.* (2001) investigated the effectiveness of airborne digital imaging, particularly colour-infrared (CIR) imagery, in identifying Phytophthora foot rot infection in citrus trees, which poses a substantial threat to the citrus industry in the Lower Rio Grande Valley in Texas, USA. By examining symptoms such as leaf yellowing and canopy defoliation, the study utilized both aerial imagery and ground-based spectroradiometric measurements to differentiate between healthy and infected trees (Fletcher *et al.*, 2001). Results showed that CIR imagery successfully distinguished between healthy and infected trees. The significance of differences between the means of healthy and infected trees for each of the captured wavelengths measured by the spectroradiometer was assessed using the unpaired Student's t-test (Fletcher *et al.*, 2001). Furthermore, differences in NIR spectral reflectance indicated promising potential for digital imaging in promptly assessing foot rot-infected citrus trees in real-time field scenarios (Fletcher *et al.*, 2001).

Extensive research has focused on studying the spectral characteristics of the red-edge concerning the differentiation of healthy and diseased lemon trees. Studies indicate that the analysis of airborne hyperspectral signatures, specifically employing red-edge position technology, proves effective in identifying diseases such as citrus greening within affected tree canopies (Li *et al.*, 2012).

2.5.2. UAV and Airborne Resolution

The integration of remote sensing, particularly through UAVs, has transformed agriculture by providing high-resolution spatial data. UAV-based remote sensing is invaluable for disease detection in trees, capturing detailed information not discernible through traditional methods. Sankaran *et al.* (2013) discussed the use of UAVs in agriculture, emphasizing their potential for monitoring plant health. The ability of remote sensing to capture multispectral data enhances its utility in detecting subtle changes associated with diseases in citrus trees (Garcia-Ruiz *et al.*, 2013). High-resolution imagery like Quickbird, SPOT, and IKONOS is costly, while medium-resolution imagery with revisiting periods of 16 days may not provide high-quality data in time for continuous fruit tree monitoring (Zhou *et al.*, 2022).

In a study conducted by Garza *et al.* (2020) on a grapefruit orchard affected by Huanglongbing (HLB) and Phytophthora foot and root rot, a UAV equipped with an RGB camera was employed to evaluate citrus health. Triangular greenness index (TGI) images generated from the UAV data were correlated with various field measurements, including tree nutrient status, leaf area, foot rot severity, and HLB presence (Garza *et al.*, 2020). Results indicated that 61% of the TGI differences could be attributed to factors such as sodium, iron, foot rot, calcium, and potassium. This study underscores the potential of UAVs with RGB cameras for monitoring diseased citrus trees, with TGI serving as a valuable tool for highlighting variations in tree health resulting from multiple diseases (Garza *et al.*, 2020).

Moreover, the accuracy of distinguishing between citrus groves infected with HLB and healthy samples exceeded 90% when employing a straightforward red edge position threshold method on the ground reflectance datasets. This held true regardless of whether the measurements were conducted in the field or indoors (Li *et al.*, 2012). However, this method proved less effective with hyperspectral airborne images due to their lower spatial resolution. In contrast, SVM analysis emerged as a viable solution and adaptable approach for constructing a mask to delineate tree canopies (Li *et al.*, 2012). Furthermore, Zarco-Tejada *et al.* (2018) has leveraged the temporal aspect of red-edge spectral indices, including Normalised Difference Vegetation Index (NDVI) and Transformed Chlorophyll Absorption Ratio Index (TCARI) normalized by the Soil Adjusted Vegetation Index (OSAVI) to assess the structural and pigment-related alterations in trees over time. Through the comparison of these indices, with a high temporal resolution, analysts can ascertain whether a tree crown is experiencing a gradual decline or sustaining a healthy state, thereby offering valuable insights into the overall health status of trees (Zarco-Tejada *et al.*, 2018).

2.5.3. Image Processing and Analysis Methods

The importance of pre-processing of multispectral orthomosaic data cannot be overstated. Valerio Giuffrida *et al.* (2022) highlighted the tasks involved in pre-processing, such as radiometric calibration, atmospheric and geometric correction. These steps are vital to ensure the reliability of the data for analysis and directly impact the accuracy of disease classification. Jay *et al.* (2019) discussed the importance of pre-processing in remote sensing applications and its impact on data quality. The accuracy of disease classification is influenced by the quality of input data, making pre-processing an essential step in the workflow (Jay *et al.,* 2019).

Statistical analyses such as the t-test for two samples and the f-test for variances play a crucial role in assessing the statistical significance of differences between datasets (Mishra *et al.*, 2019). In the context of this study these statistical tests provide possible spectral separability between the different crop health conditions. The t-test is particularly relevant when comparing means of two independent samples, such as evaluating the performance of disease detection models in different scenarios. Meanwhile, the f-test aids in determining if the variances of two datasets are significantly different, which is essential in understanding the data collected (Mishra *et al.*, 2019).

A statistical analysis can also be performed with JMP 13.0.0 (JMP LLC, USA) to explore the relationship between UAV image and field data (Garza *et al.*, 2020). Specifically, a multivariate correlation function within JMP was employed to establish pairwise and higher-order relationships among nutrient concentrations, physiological parameters, and TGI (Garza *et al.*, 2020). To discern statistical differences between disease classifications, nutrient status, and TGI for each measured factor, a full factorial analysis was conducted, with mean separation determined using the Student's t-test ($p \leq 0.05$) (Garza *et al.*, 2020).

2.5.4. Deep Learning for Detecting Disease in Fruit Trees

Deep learning models have revolutionized image classification tasks in agriculture, offering unprecedented capabilities in various applications, from crop monitoring to disease detection. ResNet-101, a deep convolutional residual neural network architecture, has gained prominence for its ability to learn intricate features from images (He *et al.*, 2015). He *et al.* (2015) introduced the ResNet architecture, emphasizing its deep residual learning approach. This architecture has been successfully employed in diverse domains, including plant disease classification. Liakos *et al.* (2018) discussed the application of deep learning in agriculture, highlighting its potential for advancing precision farming practices and addressing challenges in crop management.

The review by Liakos *et al.* (2018) highlights the potential of deep learning in advancing precision farming practices. The application of ResNet-101 in plant disease classification, as demonstrated by Mohanty *et al.* (2016), highlights its ability to differentiate subtle visuals indicative of diseases, offering an approach for early and accurate detection. Deep learning models offer a promising avenue for the detection process, which can be incorporated into the disease management strategies (Deng *et al.*, 2020). Furthermore, the use of deep learning algorithms in conjunction with UAVs has enabled the detection of various diseases and pests in fruit trees with high accuracy. For example, studies on orchard monitoring demonstrated successful disease detection outcomes, such as identifying infected or diseased trees, which had citrus bacterial canker in different disease development stages (Popescu *et al.*, 2023). These applications have shown promising results in terms of accuracy, with detection rates ranging from 81.67% to 100% for different diseases (Popescu *et al.*, 2023).

Sarkar et al.'s (2016) study on citrus greening using UAV mounted sensors, which employed machine learning models to distinguish between healthy and infected leaves of orange trees, achieved validation accuracies as high as 93%. These models included linear and standard gaussian SVM.

2.5.5. Limitation of Remote Sensing for Detecting Disease in Fruit Trees and Research Gaps

Research gaps exist in data fusion techniques, which play a vital role in integrating data from multiple sensors to enhance disease detection capabilities in crops and fruit trees (Jafarbiglu and Pourreza, 2022). Further research is needed to enhance feature extraction methods to improve the identification and differentiation of disease symptoms in fruit trees using remote sensing technologies (Jafarbiglu and Pourreza, 2022). There are research gaps in sensor calibration methodologies, which is crucial for ensuring the accuracy and reliability of remote sensing data for disease detection in fruit trees (Jafarbiglu and Pourreza, 2022). Simply analysing changes in spectral reflectance and vegetation indices may not be sufficient to accurately classify fruit tree healthy status, especially when dealing with complex planting structures and uneven orchards (Zhou *et al.*, 2022).

The current literature offers valuable insights into deep learning applications for disease detection in plants, including citrus trees. While the sources focus on citrus pests and diseases, there is no specific mention of remote sensing approaches identifying *Phytophthora spp*. in lemon trees. The studies demonstrate the success of deep learning models in classifying citrus pests and diseases, showcasing the potential of artificial intelligence in agriculture. Therefore, there is a need to evaluate deep learning methods related to Phytophthora in lemon trees. Further research focusing on this particular disease and citrus is necessary. The existing studies lay a foundation for utilizing deep learning techniques in plant disease detection, including citrus diseases, and highlight the importance of advanced technologies in enhancing agricultural practices.

Chapter 3: Methods

3.1. Study Area

The study area is a lemon farm located in Marble Hall, Limpopo, South Africa. The coordinates of the study area are 25.086287 S and 29.204630 E. This region is characterized by its vast agricultural landscape, with a significant presence of lemon orchards. The selection of Marble Hall was influenced by the prevalence of root rot in lemon trees, a condition that poses a substantial threat to citrus production in the area. The region exhibits a semi-arid climate and lies within the summer rainfall zone, where average daily high temperatures surpass 23 °C in winter (June to August) and 29 °C in summer (December to February). The average annual precipitation is approximately 635 millimetres (Maponya and Mpandeli, 2012). Furthermore, the 12.5 ha spatial extent of the study area (field F7) in Figure 1 is mostly flat terrain.

The study covers a specific portion of Marble Hall. El Sundew, a company which supplies most of the lemons and oranges to South African grocery stores was chosen as the study area due to access and disease presence in their lemon tree field. A few trees within field F7 were carefully inspected for root rot caused by phytophthora, which is the common disease identified yearly in this field (Jaouad *et al.*, 2020). This area was chosen due to the known occurrence of root rot, making it an ideal site to investigate and develop a model for early detection. Root rot is a common disease affecting citrus trees globally, causing significant economic losses. Understanding its spread and identifying affected trees quickly can aid in implementing targeted management strategies.

Lemon trees thrive in warm temperatures, but extreme heat or cold stress can weaken the trees, making them susceptible to diseases like root rot (Jaouad *et al.*, 2020). Root rot is associated with excessive soil moisture and poor drainage which creates a favourable environment for the spread of root rot pathogens (Jaouad *et al.*, 2020). High humidity can contribute to the spread of fungal diseases, including root rot. Proper ventilation and spacing between trees can help reduce humidity levels (Jaouad *et al.*, 2020).

The farm incorporates the following agricultural practices. An automated irrigation system that delivers water to the base of each individual tree. This system applies a fixed amount of water at fixed time intervals throughout the day. However, there is no soil moisture sensor, which can increase the risk of over or under-irrigation as the climatic conditions vary day to day. Pesticides and fungicides are manually sprayed onto the trees row by row every two weeks. The lemon trees are planted three metres apart to promote good air circulation. Root rot is often caused by pathogens in the soil, such as *Phytophthora spp.* (Nagle *et al.*, 2013). These pathogens may be dormant in the soil, waiting for favourable conditions to infect tree roots. Once infected, the roots may rot, leading to symptoms like wilting and yellowing of leaves. This ultimately results in the tree's decline. The farm removes infected trees, making sure to remove the roots entirely and replants a new tree in the same position. However, there still remains a risk that the pathogens remain in the soil which can infect the newly planted tree (Savita and Nagpal, 2012).

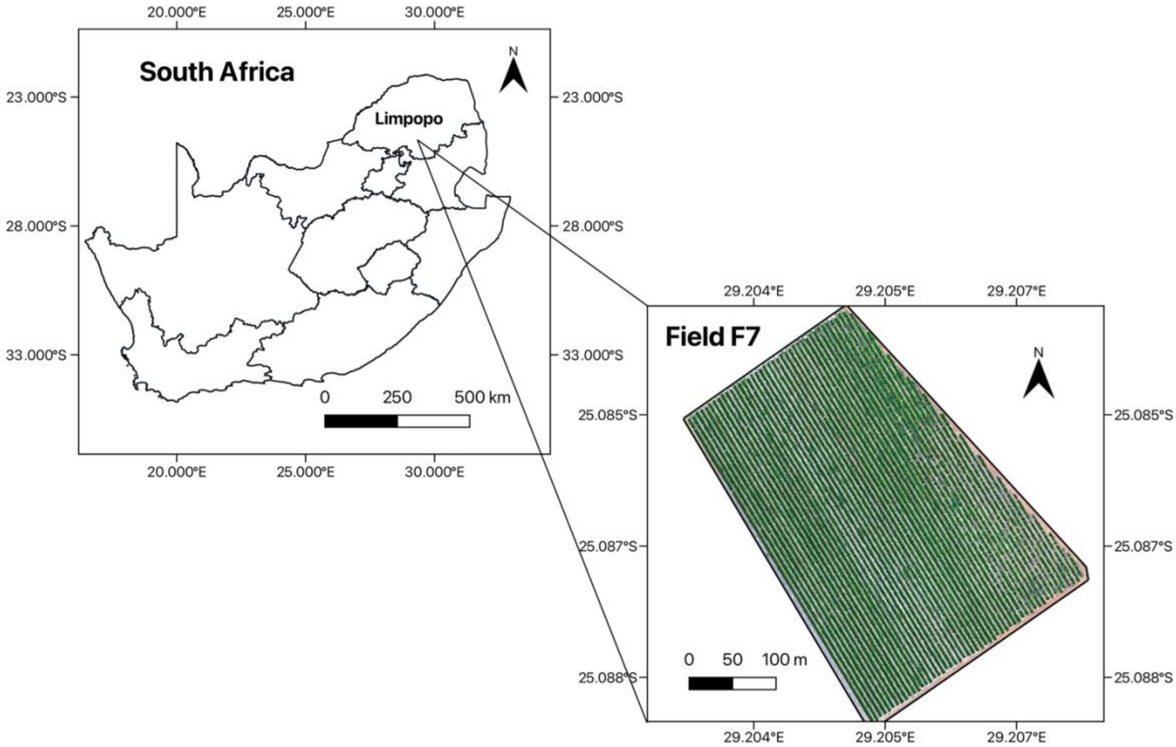

Figure 1: Map of South Africa showing the provincial boundaries as well as the location of field F7 within Marble Hall in the Limpopo province. Map of field F7 showing a high resolution RGB orthomosaic (4cm) acquired from the UAV.

Root rot is typically caused by pathogenic fungi in the soil, exacerbated by factors such as poor drainage, overwatering, and suboptimal soil conditions. In the Marble Hall region, the disease's prevalence may be influenced by a combination of climate, soil composition, and agricultural practices (Jaouad *et al.*, 2020).

3.2. Identifying Root Rot Symptoms

The following symptoms were observed in field F7 and identified as being caused by root rot using a visual inspection with the expertise of the agricultural manager at the farm. Visual inspection of the lemon tree canopies were conducted. Inspection of the tree trunks near the ground for areas of dead or damaged bark, commonly referred to as cankers, provided evidence of root rot affecting the lower parts of the tree. The presence of yellow leaves, particularly in the lower canopy, was a sign of reduced vitality. A noticeable reduction in the number of leaves and canopy thinning was observed on trees with root rot. Trees with a root rot infection, exhibited stunted growth characteristics such as thin, underdeveloped trunks and smaller canopy volume (Jaouad *et al.*, 2020). The following images show examples of the symptoms that were observed on trees that were labelled as having root rot within the samples collected. Trees which did not exhibit these symptoms, were labelled as healthy.

El Sundew, the farm which manages the lemon orchards performs regular soil analyses to determine the pathogens responsible for the symptoms observed. The lab results for the 2023 growing season confirm that the pathogen responsible for the symptoms was Phytophthora.

Figure 2: Photograph showing a lemon tree infected with root rot showing symptoms of cankers surrounding the trunk

Figure 3: Photograph showing a declining lemon tree infected with root rot showing symptoms of yellow leaves and noticeable leaf drop and sparse foliage.

Figure 4: Photograph showing a healthy lemon with a dense canopy showing no visible symptoms of root rot infection.

Table 1: Summarising the common symptoms caused by Phytophthora root rot in lemon trees

Symptom	**Description**
Yellowing leaves	Lack of vitality and yellow leaves in lower canopy
Leaf drop	Reduction in foliage and canopy thinning
Stunted growth	Diseased tree may have shorter branches, smaller leaves and trunks compared to healthy trees
Wilting	Root rot affects the ability of the tree to absorb water and nutrients, leading to dehydration
Cankers	Dead or damaged bark near the ground
Root decay	Discoloured and foul odour when roots dug up

3.3. Data Acquisition

3.3.1. UAV and Sensor Information

Data collection involved the use of a UAV platform (DJI Matrice 300) equipped with a MicaSense RedEdge-P sensor. The UAV provided high-resolution imagery, and the sensor captured data in multiple spectral bands (red, green, blue, red edge, and near-infrared), enhancing the ability to detect subtle variations in plant health (Dash *et al.*, 2017). This sensor also features a high resolution panchromatic band, which was applied to each band individually to pan sharpen, which increases their resolution and clarity (Jenerowicz and Woroszkiewicz, 2016). Pan sharpening is part of the pre-processing workflow. The multispectral sensors have a resolution of 1.58 MP and the panchromatic sensor has a resolution of 5.1 MP, this results in the multispectral sensors having approximately half the GSD at any given height when compared to the panchromatic sensor. The centre, bandwidth and GSD of each band recorded by the sensors are shown in Table 2:

Table 2: Showing the centre, bandwidth and GSD for each band captured by the Micasense RedEdge-P sensor (MicaSense Knowledge Base, 2021)

Bands	Centre (nm)	Bandwidth (nm)	GSD at 120 m (cm)
B1 - Blue	475	32	7.7
B2 - Green	560	27	7.7
B3 - Red	668	16	7.7
B4 - Red edge	717	12	7.7
B5 - Near infrared	842	57	7.7
B6 - Panchromatic	634.5	463	3.98

Additionally, the global navigation satellite system (GNSS) on the UAV recorded GPS coordinates for each captured image, facilitating the geotagging of raw images. The UAV platform had Real Time Kinematics (RTK) enabled and utilised the DJI GNSS-RTK base station to accurately correct in real time the position (x, y and z axis) of the images captured by the UAV. The UAV sensor was placed over calibrated reflectance panels before each flight to accurately calibrate the sensor to ensure accurate surface reflectance values while utilising the additional sunlight sensor connected to the MicaSense RedEdge-P. Accurate surface reflection data can be expected and is important to capture small deviations in the trees spectral signatures.

UAV data was preferred over freely available Sentinel or other satellite data due to its higher spatial resolution, flexibility in flight planning, and the ability to capture specific areas of interest in a timely manner. This level of detail is crucial for accurately identifying and monitoring individual lemon trees affected by root rot (Pádua *et al.*, 2020). One major advantage of UAV data is that it is not sensitive to cloud cover and additional atmospheric correction during the pre-processing stages is not required (Fei *et al.*, 2022). This UAV based remote sensing approach allows for mapping of large areas per flight while enabling detection of early disease in trees that could have been missed by manual field scouting. Therefore, this approach allows for timely, efficient and less laborious mapping when compared to manually inspecting each tree in the field (Günder *et al.*, 2022).

3.3.2. Flight Plan Settings

The DJI Pilot 2 app, installed on the DJI smart transmitter was used to plan the flights and used for real time flight management. The UAV flights were planned to cover the designated field, with appropriate overlap (75% horizontal and 75% vertical) to ensure sufficient coverage. Flight planning parameters included an altitude of 120 m above ground, flight speed of 15 m/s. The camera angle was set to 90 degrees also known as nadir. The flights were conducted on the 3rd of October 2023 between 12 pm and 2 pm ensuring optimal weather conditions for image capture. There was no cloud cover and full sun shine.

Overlapping imagery is crucial for creating accurate and detailed maps of the surveyed area. A higher overlap (75%) ensures that each area is captured from multiple perspectives, minimizing the risk of information gaps or inconsistencies in the dataset. Studies completed by Dandois *et al.*, (2015) have shown that a high overlap improves the accuracy of image stitching and 3D reconstruction, essential for precise analysis of plant health.

An altitude of 120 meters provided a good balance between achieving a sufficient ground resolution and covering a larger area per image, thus reducing the total number of images needed for complete coverage. This enhances the efficiency of data collection and processing. According to research by Anderson and Gaston, (2013) the choice of altitude significantly influences the resolution of remotely sensed data, and an altitude of 120 meters is often considered optimal for capturing detailed information for precision agriculture. A moderate flight speed of 15 meters per second allows for efficient data acquisition without compromising image quality. It balanced the need for fast coverage with the requirement for high resolution imagery. Research by Maes and Steppe, (2019) suggests that a moderate flight speed is suitable for obtaining accurate and reliable data, especially when dealing with unpredictable environmental conditions like wind. A moderate flight speed during image capture also minimises the risk of image distortions.

3.4. Ground Truth Data Collection

A handheld GPS device (Garmin eTrex 20) was utilized to record the precise geographic locations of the healthy and root rot infested trees within the designated rows. This ground truth dataset serves as the basis for training, validating and testing the ResNet-101 deep learning model. Trees were visually inspected for root rot symptoms with the aid of the agricultural expert on site. Trees which exhibited at least one of the symptoms were labelled as root rot. This was the approach taken in the study by Casady and Palm, (2002) on remote sensing and ground truth procedures. Trees which did not show any visible symptoms were labelled as healthy. In total 46 samples were collected for root rot infested trees and 46 samples were collected for healthy trees. The samples were randomly distributed throughout the field.

An equal number of samples were collected for both root rot and healthy trees. This balance is crucial for statistical comparisons and minimizing biases in the analysis. A total of 36 samples were randomly selected from each group to form the training dataset. The remaining 10 samples in each group was used as the test dataset. This created an approximate 80/20 percentage split for the training and test datasets. This resulted in a total of 72 samples in the training set and 20 samples in the test set. To increase the reliability of results, 5-fold stratified cross validation was utilised during model training.

The point data from the Garmin handheld GPS was visualised in QGIS 3.34.4 LTR (QGIS Development Team, 2023) and overlayed on top of the processed orthomosaic. In QGIS, circular polygons were manually created to delineate each tree of interest and assigned the appropriate class labels. The choice of circular polygons was preferred over rectangular boxes. When utilizing a box to delineate trees, it results in a larger area of ground being included in the image, which is undesirable for comparing the spectral signatures of healthy and root rot-infested trees (Poláček *et al.*, 2022). The circular shape focuses on the central region of interest, minimizing the inclusion of irrelevant background information. This can be beneficial when the object of interest is centrally located within the image, reducing the influence of surrounding context (Poláček *et al.*, 2022). In this case where the objects to be classified are naturally circular, using circular masks helps the model better conform to the inherent shape of the objects. This can enhance the model's ability to capture and learn relevant features. Research by Pádua *et al.*, (2020) on ink disease in chestnut trees, utilised individual tree crown detection within the workflow of classifying trees that were healthy or diseased. This tree crown detection was automated in their research, but for the purposes of this study, the tree crowns were manually masked for training purposes. This was repeated for all 46 healthy and 46 root rot infested samples and each mask was assigned the corresponding class.

Opting for circular polygons is advantageous because, compared to a box shape encompassing the same tree, there are fewer pixels within the polygon (Poláček *et al.*, 2022). This reduction in pixels allows for more effective feature extraction in deep learning models, as reshaping the image tile to fit the model's input size leads to less loss of information (Poláček *et al.*, 2022). Figure 5 shows an example of one healthy and one root rot infested tree.

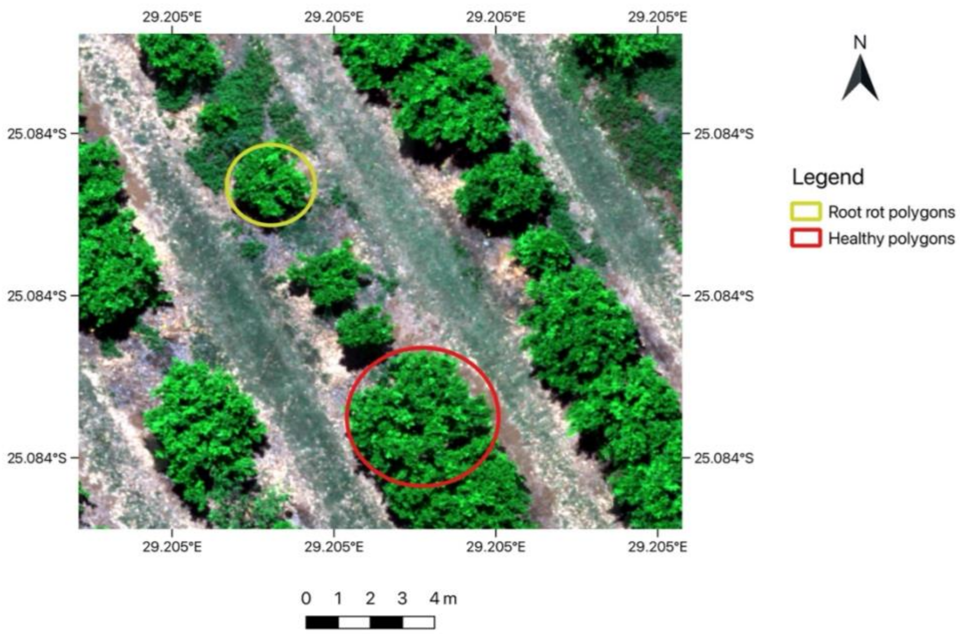

Figure 5: Orthomosaic showing an extract of the masks manually created to delineate the trees in the training and test datasets which were used for model training and testing.

3.5. Pre-Processing of UAV Images

Pre-processing of the UAV images involved orthorectification, which is the process of removing image distortions such as sensor tilt and topographic relief when stitching the images together to create an orthomosaic (Habib *et al.*, 2016). UAV images often exhibit geometric distortions due to variations in terrain and the flight path of the drone. Orthorectification corrects these distortions, ensuring that the image is georeferenced accurately (Habib *et al.*, 2016). This spatial accuracy is essential for precise identification and mapping of disease patterns in the field. Radiometric calibration standardizes the pixel values across different images, accounting for variations in illumination conditions during UAV flights. This step is crucial for ensuring that pixel values accurately represent the reflectance or radiance of the objects in the scene, allowing for consistent analysis (Guo *et al.*, 2019). Radiometrically calibrated images enable quantitative analysis of spectral information. This is vital for detecting subtle changes in tree health and identifying disease specific spectral signatures.

These pre-processing steps are crucial for maintaining pixel accuracy and reliability. Without these pre-processing steps, the resulting orthomosaic may exhibit distortions in the shape of the trees as well as large errors in the surface reflection across the orthomosaic, as multiple UAV flights were required (Popescu *et al.*, 2023). Before pan-sharpening, it's crucial to ensure that the panchromatic and multispectral images are correctly aligned or registered. Image registration involves geometrically aligning the pixels of the different image bands using key point matching so that corresponding features are spatially aligned (Kumar Mishra, 2012). This was performed by the photogrammetry software Pix4DFields 2.2.2 (Pix4D, Switzerland) . This pre-processing step is required as it allows for accurate and reliable analysis of the resulting orthomosaic.

The panchromatic band has a higher spatial resolution compared to the multispectral bands. The first step of pan-sharpening is to increase the spatial resolution of the multispectral bands to match that of the panchromatic band (Jenerowicz and Woroszkiewicz, 2016). This was be done using resampling, which is an interpolation technique. Various algorithms are used for pan-sharpening, however the method used by the photogrammetry software Pix4DFields is the Brovey Transform. This transformation has the advantage of preserving the colour information of the original multispectral bands, as it aims to maintain the spectral characteristics of the input multispectral data. The Brovey Transform is relatively simple computationally compared to some other pan-sharpening methods, making it computationally efficient (Jenerowicz and Woroszkiewicz, 2016). This method has been used historically in remote sensing applications and is well-established.

The Brovey Transform is a linear colour normalization method that scales the intensity values of each multispectral band based on the ratio of the panchromatic band intensity at each pixel (Jenerowicz and Woroszkiewicz, 2016). Image registration and pan-sharpening contribute to the construction of a multispectral orthomosaic with improved spatial and spectral information, enabling more accurate tree classification (Jenerowicz and Woroszkiewicz, 2016). The bands; red, green, blue, red-edge and NIR for each UAV image were pansharpened before they were stitched together to create the orthomosaic using Pix4DFields. The geographic coordinate system used was WGS 1984, and the projected coordinate system used was WGS 1984 Transverse Mercator. The resulting spatial resolution of the multispectral orthomosaic was 4 cm. The orthomosaic is now ready for further analysis.

3.6. T-Test and F-Test for Spectral Band Differences

Both the t-test and f-test assume the data within each group is approximately normally distributed. If the sample sizes are sufficiently large (typically, $n > 30$), the central limit theorem often ensures normality. The other assumption is of independence, where observations within each group should be independent of each other (Mishra *et al.*, 2019). To determine if there is a significant difference in average mean values between healthy and diseased lemon trees for each of the five spectral bands recorded by the MicaSense RedEdge sensor, a t-test for two independent groups was employed. This statistical test assesses whether the means of two groups are significantly different from each other. First an f-test was performed for each of the five spectral bands to determine if the two groups variances were statistically equal or unequal as this will determine the correct t-test to use (Gastwirth *et al.*, 2009). The results of the t-test is presented in a table.

For each spectral band (red, green, blue, red edge and NIR) the mean values for healthy and diseased tree samples were calculated in the following manner. Each of the 46 polygons for both classes were used to clip the orthomosaic. Zonal statistics were calculated for each polygon (sample) using the raster processing tool in QGIS and exported to Excel (Microsoft Inc., 2020). This included the mean pixel value for each band in the orthomosaic for each sample. This is plotted in the results section. The results provide insights into which spectral bands are most indicative of the presence of root rot in lemon trees using traditional statistical approaches. This highlights the advantages of deep learning which is able to extract more complex features of objects within images. Both the t-test and f-test were performed using the data analysis function in Excel.

This comprehensive evaluation, combining accuracy metrics and statistical tests for spectral bands, ensures a thorough understanding of the deep learning model's performance and provides insights into the spectral characteristics associated with root rot in lemon trees.

3.7. Modelling

3.7.1. Resnet-101 Model Overview

The deep learning model employed in this research is the ResNet-101 architecture, developed by Microsoft Research in 2015 (He *et al.*, 2015). ResNet, short for Residual Network, is renowned for its ability to handle complex image recognition tasks. ResNet-101 specifically consists of 101 layers, utilizing residual connections to mitigate the vanishing gradient problem (increasing error when training deeper layers), allowing for a more effective training of deep networks (He *et al.*, 2015). The advantage of adding this type of skip connection is that if any layer negatively impacts the performance of the model, it is skipped by a process called regularization. This process ensures the number of parameters to train the model also remains less than other common deep neural network architectures (He *et al.*, 2015).

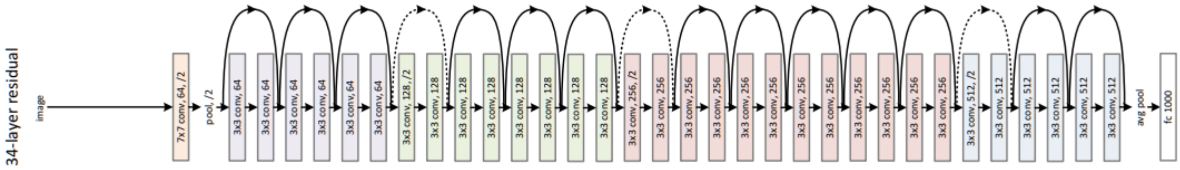

Figure 6: Diagram showing the structure and layers of the ResNet-34 model, highlighting the residual connections that are also utilised in the ResNet-101 model (He et al., 2015).

Figure 6 shows the structure of ResNet-34. ResNet-101 structure is similar and includes more layers. The following layers within the model are described below. In Figure 7, the initial convolutional layer processes the input images to extract low-level features. The 7x7 kernel size with 64 filters and a stride of two helps capture basic patterns and structures. Batch normalization normalizes the output of the convolutional layer, which helps in stabilizing the training process. Non-linearity is introduced through the rectified linear unit (ReLu) activation function.

ResNet-101 comprises a total of 104 convolutional layers organized into 33 convolutional blocks. Among these blocks, 29 utilize the output of the preceding block directly through a residual connection. The remaining four blocks take the output of the previous block, process it through a convolution layer with a filter size of 1x1 and a stride of one, and then apply a batch normalization layer (Demir *et al.*, 2019). The global average pooling layer condenses the spatial dimensions of the feature maps into a single value per feature map. This process aids in decreasing the overall number of parameters in the network by reducing the size of the image input to the model (Demir *et al.*, 2019). The classification layer (Softmax) produces the final output probabilities for different classes. In classification tasks, this layer maps the extracted features to class probabilities.

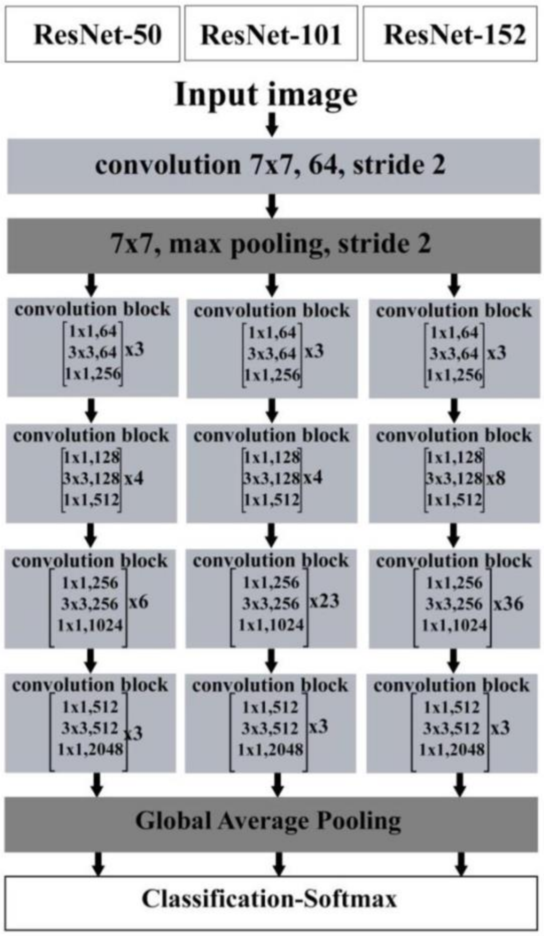

Figure 7: Structure of the different layers within the ResNet-101 model (He et al., 2015).

3.7.2. Transfer Learning

The upper layers of the model, especially those responsible for task specific classification, undergo fine tuning on the new dataset. These layers adapt to the unique characteristics of the dataset. The ResNet-101 model, originally pretrained on the large ImageNet dataset consisting of 1 million images (ArcGIS Pro Documentation, 2023), comes with precalculated weights for its three trained channels: red, green, and blue. However, since the new dataset includes the multispectral channels red-edge and NIR, random initial weights are assigned to them and adjusted with each training epoch. Research by Gadiraju and Vatsavai, (2020) has shown promising performance when selecting randomly initialised weights for deep transfer learning for crop classification.

In typical transfer learning scenarios, the feature extraction layers, usually lower and middle layers, are often frozen. This means that the model retains the knowledge acquired from the extensive ImageNet dataset, and these layers are not updated during fine-tuning on the smaller dataset. Freezing is beneficial for preserving generic features from pre-training (Rai and Flores, 2021). However, in this case, the layers were not frozen, allowing the model to adapt and classify images more precisely. This decision involves a trade-off in computation time, as estimating more parameters becomes necessary.

3.7.3. Key Benefits of Transfer Learning

Transfer learning offers several advantages. It accelerates convergence during fine-tuning since the model begins with weights that already capture useful features. Generalization is improved because the pre-trained weights assist the model in adapting better to the new task, even when labelled data is limited. Additionally, there is a reduced need for annotated data, making transfer learning particularly valuable when the new dataset is small and lacks sufficient labelled examples (Nowakowski *et al.*, 2021). Given its success in image classification tasks, especially in agriculture, this architecture is a suitable choice for identifying root rot in lemon trees within the Marble Hall region.

3.8. Training Resnet-101 Model

The ResNet-101 model was trained on the pre-processed drone imagery using the ground truth dataset. Bounding polygons around the lemon trees were manually created and labelled as healthy or root rot. These labels were used as training labels for the model. A total of 36 samples for each tree class were used for training, while the remaining 10 samples for each tree class were set aside for the testing dataset. Before the model was trained, the bounding polygon surrounding each sampled tree was used to create an image tile of size 448 by 448 pixels with the appropriate class label. The training data was stored and organised as follows; the healthy tree labelled tiles were stored in a separate folder to the root rot tree labelled tiles. The ImageNet format was used to save the .tif image tiles and corresponding .tfw file. A value of zero (0) was assigned to root rot tiles and a value of one (1) was assigned to healthy tiles.

Before the tiles were inputted for training they were all resized to 224 by 224 pixels which is the recommended size for the pretrained ResNet-101 model (He *et al.*, 2015). Any pixels with no data values were set to zero. The pixels in an image usually range from 0 – 255 however in this case they were already normalised from the Pix4DFields software which resulted in each band having a minimum of zero and maximum of one.

Data augmentation involves artificially expanding the training set by generating modified versions of the image tiles, particularly when the dataset is limited in size (Taylor and Nitschke, 2018). The following augmentations were randomly applied to the image tiles; rotation by 45 degrees, cropping, dihedral affine, brightness, contrast, and zoom. These augmented image tiles were appended to the original training data to increase the training sample size.

The training process involved iteratively adjusting the model's parameters to minimize training and validation losses which resulted in decreasing classification errors with each epoch (Ghosal *et al.*, 2019). While training the neural network, 10% of the training data was used as a validation dataset. This allowed one to view the validation error for each epoch. 100 epochs were used for training. The model’s parameters were pretrained on the ImageNet dataset. The layers were unfrozen to allow adequate fitting of the model to the healthy and diseased tree images. The batch size used was eight, to prevent any memory errors while training. The computer used for training utilised an AMD Ryzen 7 5700X 8-core CPU and Nvidia GeForce GTX1660 Super 6GB GPU. The training time took approximately 30 minutes using the GPU for the training. The training was initially performed on the CPU as a benchmark and took considerably longer at 6 hours. Therefore, it is recommended to perform deep learning training on GPU hardware when available (Wang *et al.*, 2019). Subsequently, the trained model was applied to the test dataset to evaluate its performance in classifying healthy and root rot infested lemon trees. Stratified 5-fold cross validation was employed to increase the reliability of the accuracy assessments. The data is presented in the form of figures and tables including a confusion matrix. The root rot spatial distribution was investigated for any patterns.

The training and validation loss was graphed in order to evaluate whether the ResNet-101 model converged during training. Convergence indicates that the model has stabilised and any further training is unlikely to significantly improve performance. This is crucial for determining an appropriate stopping point to avoid overfitting (Ghosal *et al.*, 2019). Monitoring the training and validation loss over epochs provides insights into the progress of the model during training. A steady decrease in the training and validation loss suggests that the model is learning from the data. Sudden increases in the validation loss, while the training loss continues to decrease, may indicate overfitting. A stable loss indicates that the model generalizes effectively to augmented data (Ghosal *et al.*, 2019).

This comprehensive methodology ensures the reliability and accuracy of the research findings, providing a robust framework for the identification of root rot in lemon trees using multispectral UAV imagery and a deep learning architecture.

3.9. Accuracy Assessment

To assess the classification performance, several accuracy metrics were utilized, including overall accuracy, recall, precision, and F1 scores. The dataset was split into approximately 80% for training and 20% for testing. Overall accuracy represents the ratio of correctly classified samples to the total number of samples across all classes, with samples derived from the multispectral orthomosaic in this study. Recall, precision, and F1 scores are computed based on true positives (TP), true negatives (TN), false positives (FP), and false negatives (FN) (Terven *et al.*, 2023). Predicting a tree as diseased is regarded as positive, while predicting a tree as healthy is regarded as negative.

The metrics were calculated as follows for each class:

$$Recall = \frac{TP}{TP+FN} \qquad (1)$$

$$Precision = \frac{TP}{TP+FP} \qquad (2)$$

$$F1\ score = \frac{2TP}{2TP+FN+FP} \qquad (3)$$

$$Accuracy = \frac{TP+TN}{TP+TN+FP+FN} \qquad (4)$$

Recall measures the model's ability to predict a diseased lemon tree when the tree is diseased. Precision measures the model's ability to correctly identify diseased lemon trees without misclassifying healthy ones. The F1 score provides a balanced measure of the model's overall performance. Accuracy offers a general overview of the model's correctness in its predictions. The above metrics will be calculated using the values from the test confusion matrix. The test confusion matrix includes all the results from all five test sets generated by using stratified 5-fold cross validation. Stratified cross validation was selected to ensure an equal class proportion of healthy and root rot in each training and test split (T R *et al.*, 2023).

3.10. Spatial Distribution

The spatial distribution of the root rot infestation was assessed by applying the trained ResNet-101 classification model to each tree in field F7. A similar approach was employed to detect the bounding polygon of the remaining non sampled trees. For this object detection task a ResNet-34 architecture was used. The trained model was applied to the entire orthophoto to detect bounding polygons for each lemon tree in the field.

Chapter 4: Results

4.1. Zonal Statistics

The average pixel value within the mask polygons for each tree group is plotted below. The average values for most of the bands are very similar with a small difference in the red-edge and NIR bands. Some of the differences can only be seen after the second decimal place in Figure 8 below.

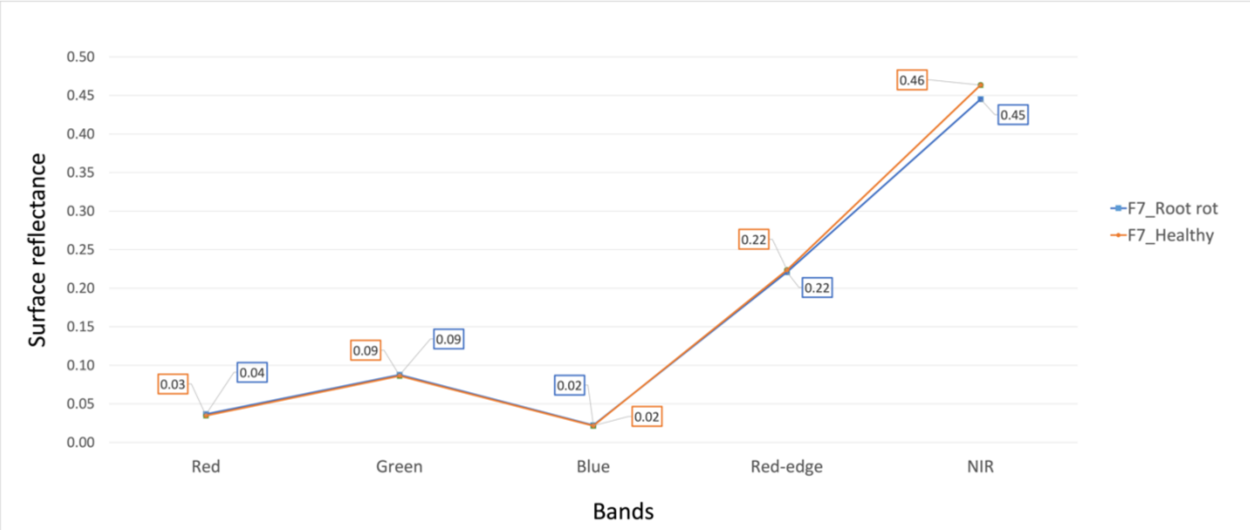

Figure 8: Plot showing the mean surface reflectance for the healthy and root rot infested tree groups in the combined training and test set for each of the five bands captured by the RedEdge-P sensor.

4.2. F-Test: Two-Sample for Variances

In order to perform the t-test, one must perform the f-test to test whether the two groups (healthy and diseased) of tree populations have equal variances for each of the five spectral bands. The results of the f-test is shown below in Table 3.

Table 3: Showing the two sided P-values and test conclusion from performing the f-test: two sample for equality of variances

Spectral band	Two sided p-value	Test conclusion
Red	0.012	Unequal variance
Green	0.080	Equal variance
Blue	0.022	Unequal variance
Red-edge	0.529	Equal variance
Near infrared (NIR)	0.228	Equal variance

From the f-tests, bands red and blue reject the null hypothesis (H0: The two groups have equal variance) in favour of the alternative hypothesis (H1: The two groups have unequal variances) at a 5% level of significance. Therefore, there is sufficient evidence to suggest that the variances differ for the red and blue bands.

The results show that, bands green, red edge and NIR fail to reject the null hypothesis at a 5% level of significance. Therefore, there is insufficient evidence to suggest that the variances differ for these bands.

4.3. T-Test: Two Sample Assuming Unequal Variances

The difference in the mean of the red and blue spectral bands for the two tree groups were tested using the t-test. The results of the t-test are in Table 4 below.

Table 4: Showing the results of performing the t-test: two sample assuming unequal variances

Spectral band	Two sided P-value	Test conclusion
Red	0.352	Equal mean
Blue	0.399	Equal mean

The results show that both the red and blue bands fail to reject the null hypothesis of equal group means, at a 5% level of significance. Therefore, there is insufficient evidence to suggest that the two means differ for the red and blue bands.

4.4. T-Test: Two Sample Assuming Equal Variances

The difference in the mean of the remaining spectral bands for the two tree groups were tested using the t-test. The two sample t-test assuming equal variances uses a pooled variance for the test statistic. The hypothesised mean difference was tested equal to zero. The results of the t-test are in Table 5 below.

Table 5: Showing the results of performing the t-test: two sample assuming equal variances

Spectral band	Two sided P-value	Test conclusion
Green	0.428	Equal mean
Red-edge	0.356	Equal mean
NIR	0.003	Unequal mean

The results show that both the green and red-edge bands, fail to reject the null hypothesis of equal group means, at a 5% level of significance. Therefore, there is insufficient evidence to suggest that the two means differ for the green and red-edge bands.

For the NIR band, the null hypothesis was rejected at a 5% level of significance. Therefore, there is sufficient evidence to suggest that the mean NIR value for the healthy and diseased trees differ. This is important as is shows that this band can contribute to the classification of different classes of trees.

4.5. Confusion Matrix

The trained ResNet-101 deep learning model was fitted to the 10 healthy trees and 10 diseased trees which were kept separate for the test dataset. This was repeated for each of the five splits in the stratified 5-fold cross validation. The results of the classification are represented in the Table 6 below.

Table 6: Confusion matrix showing healthy and root rot predictions for the test set and the calculated true positive, false positive, true negative and false negative metrics.

Predicted \ Actual	Root rot	Healthy	
Root rot	**39**	**11**	**50**
Healthy	**7**	**35**	**42**
	46	**46**	**92**

4.6. Accuracy Assessment

The accuracy metrics were calculated using the confusion matrix above. The results can be seen in Table 7 below.

Table 7: Showing the accuracy assessment for the healthy and root rot classes from the confusion matrix based on the test datasets.

Class	Precision	1 - Precision	Recall	1 - Recall	F1 Score	Overall accuracy
Root rot	0.78	0.22	0.85	0.15	0.81	0.80
Healthy	0.83	0.17	0.76	0.24	0.80	

The training and validation loss can be observed to decrease and stabilise after 100 epochs in Figure 9 below.

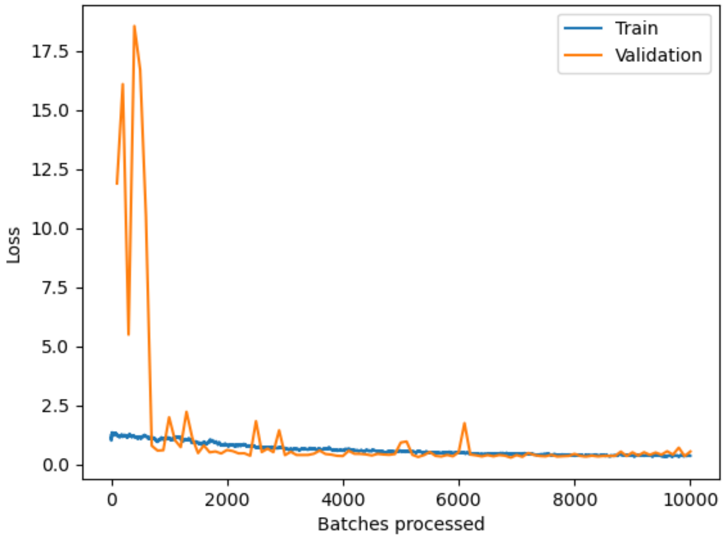

Figure 9: Graph showing the stabilisation of the training and validation loss while training ResNet-101 using the augmented training dataset.

4.7. Spatial Distribution

Figure 10 shows the spatial distribution of all the lemon trees in field F7. Yellow polygons represent trees with root rot and red polygons represent healthy trees.

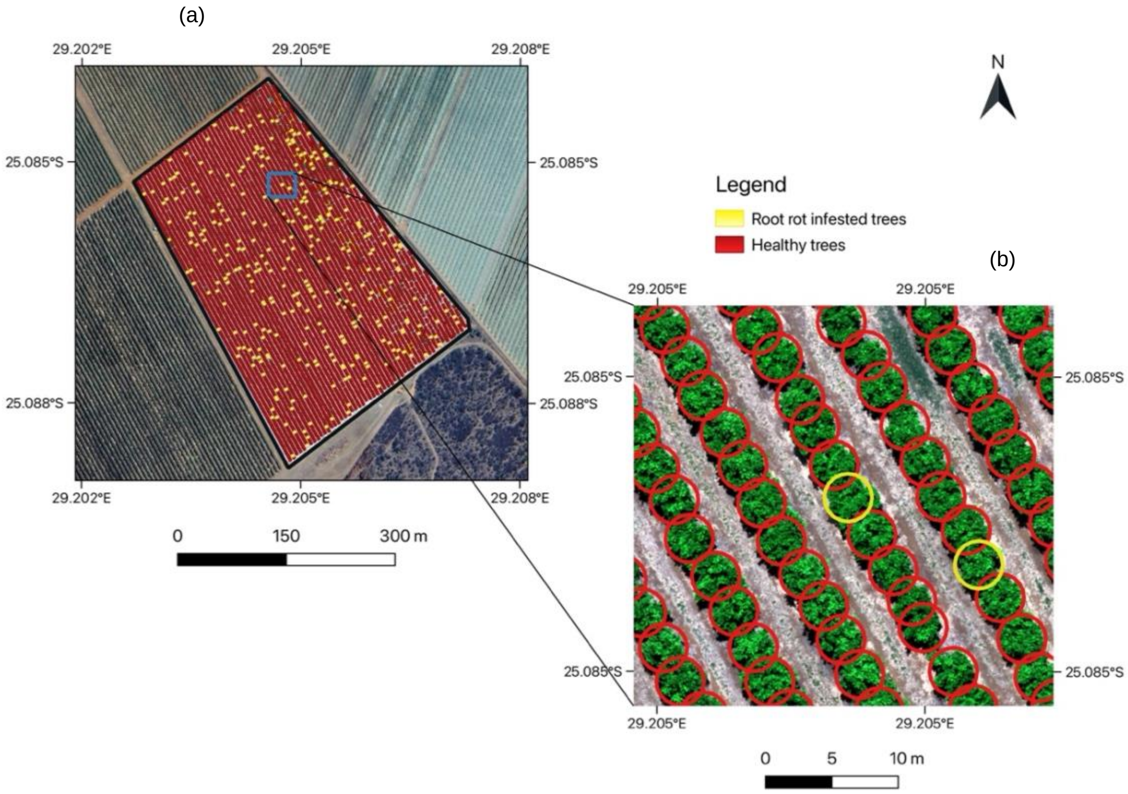

Figure 10: Map (a) showing the predicted spatial distribution for the healthy and root rot infested trees within field F7, after applying the classification model to each individual tree polygon. Map (b) showing a zoomed in extract of the map.

Chapter 5: Discussion

5.1. Spectral Characteristics of Root Rot

The zonal statistics plot presented by Figure 8 offers an insight into the variations in average surface reflectance across multiple spectral bands for healthy and root rot-affected lemon trees. The analysis focused on the bands commonly used in remote sensing applications, namely red, green, blue, red-edge, and NIR.

The average surface reflectance in the red band exhibited very similar values between healthy and root rot affected lemon trees. Physiological changes occurring in the lemon tree leaves affected by root rot, are known to alter the chlorophyll content and overall, increase reflectance in the red region (Park *et al.*, 2023). However, the mean difference was tested at a 95% level of confidence and was found to be non-significant. These results can be compared to those published by Fletcher *et al*. (2001).

Similar to the methods employed in this study, Fletcher *et al.* (2001) surveyed grapefruit trees through both aerial imagery and ground-based spectroradiometric measurements to differentiate between healthy and infected trees. Additionally, the statistical analysis using the unpaired Student's t-test found the spectroradiometric readings in the red region, revealed no significant statistical differences between the healthy and infected trees (Fletcher *et al.*, 2001).

Similar to the red band, the green band reflected significant differences between healthy and root rot-affected lemon trees. Healthy lemon trees demonstrated a lower average surface reflectance in the green band. Root rot can cause a reduced chlorophyll concentration and compromise photosynthetic processes (Park *et al.*, 2023). However, the mean difference was tested at a 95% level of confidence and was found to be non-significant. These results can be compared to those by Fletcher *et al.* (2001) which found the green spectroradiometric readings revealed no significant statistical differences between the healthy and infected trees.

The average surface reflectance in the blue band exhibited similar values between healthy and root rot affected lemon trees, with healthy lemon trees exhibiting lower average reflectance compared to the root rot sample. The blue band is known to be sensitive to changes in leaf structure and health (Gitelson *et al.*, 2003). The slightly increased reflectance in root rot trees suggests potential alterations in leaf morphology. The mean difference between the two tree groups was tested at a 95% level of confidence and was found to be non-significant. These results can be compared to those by Fletcher *et al.* (2001) which found the blue spectroradiometric readings revealed no significant statistical differences between the healthy and infected trees.

Airborne multispectral and hyperspectral images of citrus groves located in Florida, USA were studied by Li *et al.* (2012) with the aim of detecting trees infected with citrus greening. Ground truthing was conducted by means of field surveys and indoor spectral measurements, to determine the infection status of trees, along with recording GPS coordinates for each tree. Both healthy and infected trees were included in the ground truthing process. Analysis of ground spectral measurements revealed distinct differences between healthy and infected canopies (Li *et al.*, 2012). Specifically, healthy canopies exhibited lower reflectance in the near-infrared range and higher reflectance in the visible range compared to infected canopies. Furthermore, there were notable variations in the red edge position between healthy and infected canopies (Li *et al.*, 2012).

The red-edge band, sensitive to vegetation health and stress, demonstrated a small difference in average reflectance between healthy and root rot infested lemon trees. Healthy trees exhibited a higher average reflectance in this band, indicating thriving vegetation and vigour (Bandyopadhyay *et al.*, 2017). Root rot trees, on the other hand, displayed lower average red-edge reflectance, indicative of stress-induced physiological changes. The mean difference between the two tree groups was tested at a 95% level of confidence and was found to be non-significant. These results can be compared to research by Li *et al.* (2012) which found the red-edge position to be significant. This could be owing to the difference in resolution between sensors and environment and background noise (Li *et al.*, 2012).

The NIR band, known for its sensitivity to canopy structure and overall plant health, revealed a trend across the studied lemon trees (Ollinger, 2011). Canopy structure refers to the physical arrangement and organization of foliage, branches, and other components within the upper layer of vegetation. It includes factors such as leaf density, distribution, orientation, and layering within the canopy. Healthy trees displayed higher average reflectance in the NIR band, whereas root rot-affected trees exhibited lower values. This aligns with the established understanding that healthy vegetation reflects more NIR radiation, due to the changes in the leaf area index, emphasizing the importance of NIR for detecting root rot (Ollinger, 2011). The mean difference between the two tree groups was tested at a 95% level of confidence and found to be significant. These findings can be contrasted with those of Fletcher *et al.* (2001), who similarly observed that NIR spectroradiometric readings were lower for infected trees compared to healthy ones (p-value ≤ 0.05). Similarly, Fletcher *et al.* (2001) noted no significant disparities in visible reflectance data between healthy and infected trees.

In comparison, using UAVs paired with an RGB sensor to calculate a vegetation index like TGI can be used to differentiate healthy and diseased trees and explain which factors contribute to these differences. Using factorial analysis, Garza *et al.* (2020) found that relationships between the mineral nutrients: potassium, sodium, calcium, iron and Phytophthora root rot infection could explain 61% of the differences in TGI. However, it is important to note that these results may vary depending on the specific conditions and parameters of each analysis.

5.2. Detecting Root Rot in the Lemon Trees

The accuracy metrics presented in Table 7, reveal precision, recall, F1-scores and overall accuracy values which are all close to 80%. This shows promising results using a sample size of 92. Other studies have used larger samples and hence have achieved greater accuracy. With a larger sample and/or increased augmentations that were applied to the training images, better results can be expected (Kuswidiyanto *et al.*, 2022). The significance of sample sizes becomes apparent in populations exhibiting significant heterogeneity or in cases where there are minimal spectral differences between healthy and diseased trees. This emphasizes the need for adequate data to train deep learning models effectively for disease detection in plants using UAV-based aerial imagery (Kuswidiyanto *et al.*, 2022). The data acquisition system primarily relies on precise drone flights and careful flight mission planning. Recent studies have demonstrated that deep learning detection techniques offer superior accuracy compared to other machine learning detection methods (Kuswidiyanto *et al.*, 2022).

At the time of writing this research report, there were no resources which used ResNet-101 for detecting Phytophthora root rot in lemon trees. Therefore, a valid comparison is made with research using the same deep learning architecture. ResNet-101, a deep residual neural network, has been utilized in the context of detecting and locating diseases in trees using UAV remote sensing technology. Specifically, Deng *et al.* (2020) employed ResNet-101 to generate feature maps from enhanced datasets for the detection and location of dead trees affected by pine wilt disease. They were successfully able to predict the spatial distribution of dead trees.

The remaining trees within field F7 were detected using ResNet-34. This approach used sometimes identified the grass and other vegetation growing between the lemon trees as a tree. This is a side note and not the main purpose of this study. Further work can be done to assess the accuracy of the detection of tree crowns, however in this study the main focus is investigating the performance of classifying the trees as either healthy or diseased.

Stabilisation of the training and validation curves in Figure 9 indicate that the model has not been overtrained. This is again verified by relatively high accuracy metrics achieved. A graph which displays a decreasing training loss and a decreasing and then increasing validation loss may be a sign that the model has been overtrained. This would result in poor accuracy on the test dataset and high accuracy on the training dataset.

The spatial distribution of the root rot disease can be seen in Figure 10. A total of 6400 lemon trees were detected and classified using the trained ResNet-101 model. 362 trees were predicted as having a root rot infestation and the remaining 6038 were predicted as healthy. The distribution is evenly spread throughout the field with no large clusters present. Often one or two trees next to a diseased tree were also classified as diseased. This indicates that the pathogen responsible for root rot within the soil can infect multiple trees if the roots of nearby trees grow into infected soils.

Chapter 6: Conclusion

6.1. Main Findings

In conclusion, this research successfully employed ResNet-101, a deep convolutional neural network architecture, to classify healthy and root rot diseased lemon trees using multispectral UAV data. The integration of advanced deep learning techniques with high-resolution spatial information proved to be a robust methodology for accurate detection of Phytophthora root rot in citrus orchards. The findings of this study contribute to the field of precision agriculture and remote sensing, showcasing the potential of leveraging deep learning models, specifically ResNet-101, for reliable disease classification. The successful implementation of this approach highlights its practical applicability in real world scenarios, offering a promising tool for citrus growers to detect and manage root rot at its early stages.

6.2. Limitations & Recommendations

While the study provides valuable insights, several limitations must be acknowledged. Firstly, the reliance on UAV data introduces challenges related to weather conditions and flight restrictions, potentially impacting the acquisition of timely and consistent datasets. Moreover, the study concentrated on a single lemon tree species, and variations in geographic location and environmental conditions may limit the applicability of the findings to other citrus-growing regions. The presence of additional diseases in the citrus orchard, might influence the accuracy of the classification model. Another limitation is the lack of research conducted using remote sensing methodologies to detect diseases specific to lemon orchards.

Due to time and resource constraints, such as only one day allocated for UAV aerial surveying and collecting ground truth data with only one assistant, only 92 samples were collected. For increased accuracy, a larger sample is required. Data captured more regularly on the same field may also yield better results for earlier detection as symptoms would be picked up as they appear, which would enhance the model by training it with different disease stages.

The following recommendations should be considered:

I. Integration of supplementary data sources, such as hyperspectral imagery, soil samples and environmental variables, to improve the accuracy of the classification model.
II. Temporal analysis by incorporating data from multiple points in time to evaluate the progression of root rot over different growth stages of lemon trees.

References

Abdulridha, J., Ampatzidis, Y., Kakarla, S. C., & Roberts, P. (2019). Detection of target spot and bacterial spot diseases in tomato using UAV-based and benchtop-based hyperspectral imaging techniques. *Precision Agriculture*, *21*(5), 955–978. https://doi.org/10.1007/s11119-019-09703-4

Abdulridha, J., Batuman, O., & Ampatzidis, Y. (2019). UAV-Based remote sensing technique to detect citrus canker disease utilizing hyperspectral imaging and machine learning. *Remote Sensing*, *11*(11), 1373. https://doi.org/10.3390/rs11111373

Amarasingam, N., Gonzalez, F., Salgadoe, A. S. A., Sandino, J., & Powell, K. (2022). Detection of White Leaf Disease in Sugarcane Crops Using UAV-Derived RGB Imagery with Existing Deep Learning Models. *Remote Sensing*, *14*(23), 6137. https://doi.org/10.3390/rs14236137

Anderson, K., & Gaston, K. J. (2013). Lightweight unmanned aerial vehicles will revolutionize spatial ecology. *Frontiers in Ecology and the Environment*, *11*(3), 138–146. https://doi.org/10.1890/120150

Bandyopadhyay, D., Bhavsar, D., Pandey, K., Gupta, S., & Roy, A. (2017). Red edge index as an indicator of vegetation growth and vigor using hyperspectral remote sensing data. *Proceedings of the National Academy of Sciences, India. Section a, Physical Sciences*, *87*(4), 879–888. https://doi.org/10.1007/s40010-017-0456-4

Barchenger, D. W., Hsu, Y., Liao, K., Lines, C. L., Lin, S., Wang, Y., Lin, T., Huang, S., Lozada, D. N., & Bosland, P. W. (2023). Rating System for Phytophthora Root Rot Influences Quantitative Trait Locus Detection and Reveals Incomplete Dominance and Duplicative Recessive Epistatic Gene Action in Capsicum annuum. *Phytopathology*, *113*(10), 1959–1966. https://doi.org/10.1094/phyto-03-23-0086-r

Bock, C. H., Cook, A. Z., Parker, P. E., & Gottwald, T. R. (2009). Automated image analysis of the severity of foliar citrus canker symptoms. *Plant Disease*, *93*(6), 660–665. https://doi.org/10.1094/pdis-93-6-0660

Casady, W. W., & Palm, H. L. (2002). Precision Agriculture: Remote Sensing and Ground Truthing. *University of Missouri--Columbia*. https://mospace.umsystem.edu/xmlui/handle/10355/9431

Chaudhary, S., Laughlin, D. A., Setamou, M., Da Graça, J. V., Kunta, M., Alabi, O. J., Crosby, K. M., Ong, K. L., & Ancona, V. (2020). Incidence, severity, and characterization of phytophthora foot rot of citrus in Texas and implications for disease management. *Plant Disease*, *104*(9), 2455–2461. https://doi.org/10.1094/pdis-07-19-1493-re

Citrus: World Markets and trade. (2024, January 25). USDA Foreign Agricultural Service. https://fas.usda.gov/data/citrus-world-markets-and-trade

DadrasJavan, F., Samadzadegan, F., Pourazar, S. H. S., & Fazeli, H. (2019). UAV-based multispectral imagery for fast Citrus Greening detection. *Journal of Plant Diseases and Protection*, *126*(4), 307–318. https://doi.org/10.1007/s41348-019-00234-8

Dandois, J. P., Olano, M., & Ellis, E. C. (2015). Optimal altitude, overlap, and weather conditions for computer vision UAV estimates of forest structure. *Remote Sensing*, *7*(10), 13895–13920. https://doi.org/10.3390/rs71013895

Dash, J. P., Watt, M. S., Pearse, G. D., Heaphy, M., & Dungey, H. S. (2017). Assessing very high resolution UAV imagery for monitoring forest health during a simulated disease outbreak. *ISPRS Journal of Photogrammetry and Remote Sensing*, *131*, 1–14. https://doi.org/10.1016/j.isprsjprs.2017.07.007

Demir, A., Yilmaz, F., & Kose, O. (2019). Early detection of skin cancer using deep learning architectures: resnet-101 and inception-v3. *2019 Medical Technologies Congress (TIPTEKNO)*. https://doi.org/10.1109/tiptekno47231.2019.8972045

Deng, X., Tong, Z., Lan, Y., & Huang, Z. (2020). Detection and Location of Dead Trees with Pine Wilt Disease Based on Deep Learning and UAV Remote Sensing. *AgriEngineering*, *2*(2), 294–307. https://doi.org/10.3390/agriengineering2020019

Dube, T., & Mutanga, O. (2015). Evaluating the utility of the medium-spatial resolution Landsat 8 multispectral sensor in quantifying aboveground biomass in uMgeni catchment, South Africa. *ISPRS Journal of Photogrammetry and Remote Sensing*, *101*, 36–46. https://doi.org/10.1016/j.isprsjprs.2014.11.001

Elizabeth, V. D. M. (2020). *Evaluation of new postharvest fungicides for the control of phytophthora brown rot* [Thesis, University of Stellenbosch]. https://scholar.sun.ac.za/items/e7571ca1-34d7-483f-b0cd-47e09309bfcf

Eskalen, A., Adaskaveg, J. E., Menge, J. A., & Ohr, H. D. (2019, January). *Phytophthora root rot*. Agriculture: Citrus Pest Management Guidelines. https://ipm.ucanr.edu/agriculture/citrus/phytophthora-root-rot/#gsc.tab=0

Fadli, A., Benyahia, H., Hussain, S., Khan, R. I., Rao, M. J., Ahmed, T., Ancona, V., & Khalid, M. F. (2022). Phytophthora-citrus interactions and management strategies: a review. *Turkish Journal of Agriculture and Forestry :*, *46*(5), 730–742. https://doi.org/10.55730/1300-011x.3038

Fei, S., Hassan, M. A., Xiao, Y., Su, X., Chen, Z., Cheng, Q., Duan, F., Chen, R., & Ma, Y. (2022). UAV-based multi-sensor data fusion and machine learning algorithm for yield prediction in wheat. *Precision Agriculture*, *24*(1), 187–212. https://doi.org/10.1007/s11119-022-09938-8

Fletcher, R. S., Skaria, M., Escobar, D. E., & Everitt, J. H. (2001). Field spectra and airborne digital imagery for detecting phytophthora foot rot infections in citrus trees. *HortScience*, *36*(1), 94–97. https://doi.org/10.21273/hortsci.36.1.94

Futch, S. H., & Graham, J. H. (2019). Field Diagnosis and management of phytophthora diseases. *EDIS*, *2005*(10). https://doi.org/10.32473/edis-hs261-2005

Gaikwad, P. N., Sharma, V., Singh, J., Sidhu, G. S., Singh, H., & Omar, A. A. (2023). Biotechnological advancements in Phytophthora disease diagnosis, interaction and management in citrus. *Scientia Horticulturae*, *310*, 111739. https://doi.org/10.1016/j.scienta.2022.111739

Garcia-Ruiz, F., Sankaran, S., Maja, J. M., Lee, W. S., Rasmussen, J., & Ehsani, R. (2013). Comparison of two aerial imaging platforms for identification of Huanglongbing-infected citrus trees. *Computers and Electronics in Agriculture*, *91*, 106–115. https://doi.org/10.1016/j.compag.2012.12.002

Garza, B. N., Ancona, V., Enciso, J., Perotto-Baldivieso, H. L., Kunta, M., & Simpson, C. (2020). Quantifying citrus tree health using true color UAV images. *Remote Sensing*, *12*(1), 170. https://doi.org/10.3390/rs12010170

Gastwirth, J. L., Gel, Y. R., & Miao, W. (2009). The impact of Levene's test of equality of variances on statistical theory and practice. *Statistical Science*, *24*(3). https://doi.org/10.1214/09-sts301

Ghosal, P., Nandanwar, L., Kanchan, S., Bhadra, A., Chakraborty, J., & Nandi, D. (2019). Brain tumor classification using RESNET-101 based squeeze and excitation deep neural network. *2019 Second International Conference on Advanced Computational and Communication Paradigms (ICACCP)*. https://doi.org/10.1109/icaccp.2019.8882973

Giachero, M. L., Declerck, S., & Marquez, N. (2022). Phytophthora root rot: Importance of the disease, current and novel methods of control. *Agronomy*, *12*(3), 610. https://doi.org/10.3390/agronomy12030610

Gitelson, A. A., Gritz, Y., & Merzlyak, M. N. (2003). Relationships between leaf chlorophyll content and spectral reflectance and algorithms for non-destructive chlorophyll assessment in higher plant leaves. *Journal of Plant Physiology*, *160*(3), 271–282. https://doi.org/10.1078/0176-1617-00887

Günder, M., Yamati, F. R. I., Kierdorf, J., Roscher, R., Mahlein, A., & Bauckhage, C. (2022). Agricultural plant cataloging and establishment of a data framework from UAV-based crop images by computer vision. *Gigascience*, *11*. https://doi.org/10.1093/gigascience/giac054

Guo, Y., Senthilnath, J., Wu, W., Zhang, X., Zeng, Z., & Huang, H. (2019). Radiometric calibration for multispectral camera of different imaging conditions mounted on a UAV platform. *Sustainability*, *11*(4), 978. https://doi.org/10.3390/su11040978

Habib, A., Han, Y., Xiong, W., He, F., Zhang, Z., & Crawford, M. M. (2016). Automated Ortho-Rectification of UAV-Based Hyperspectral Data over an

Agricultural Field Using Frame RGB Imagery. *Remote Sensing*, *8*(10), 796. https://doi.org/10.3390/rs8100796

He, K., Zhang, X., Ren, S., & Sun, J. (2015). Deep residual learning for image recognition. *arXiv (Cornell University)*. https://doi.org/10.48550/arxiv.1512.03385

International Trade Centre (ITC). (n.d.). *Trade Map - Trade statistics for international business development*. Copyright © 2008-2014 International Trade Centre. All Rights Reserved. https://www.trademap.org/Index.aspx

Jafarbiglu, H., & Pourreza, A. (2022). A comprehensive review of remote sensing platforms, sensors, and applications in nut crops. *Computers and Electronics in Agriculture*, *197*, 106844. https://doi.org/10.1016/j.compag.2022.106844

Jaouad, M., Moinina, A., Ezrari, S., & Lahlali, R. (2020). Key pests and diseases of citrus trees with emphasis on root rot diseases: an overview. *Moroccan Journal of Agricultural Sciences*, *1*(3), 149–160. https://www.researchgate.net/publication/340515634

Jay, S., Baret, F., Dutartre, D., Malatesta, G., Héno, S., Comar, A., Weiss, M., & Maupas, F. (2019). Exploiting the centimeter resolution of UAV multispectral imagery to improve remote-sensing estimates of canopy structure and biochemistry in sugar beet crops. *Remote Sensing of Environment*, *231*, 110898. https://doi.org/10.1016/j.rse.2018.09.011

Jenerowicz, A., & Woroszkiewicz, M. (2016). The pan-sharpening of satellite and UAV imagery for agricultural applications. *Proceedings of SPIE, the International Society for Optical Engineering/Proceedings of SPIE*. https://doi.org/10.1117/12.2241645

JMP Statistical Software (13.0.0). (2021). [Software]. https://www.jmp.com/en_us/software/data-analysis-software.html

Joubert, D., & Labuschagne, N. (1998). Effect of soil compaction on Phytophthora nicotianae root rot in rough lemon and troyer citrange citrus seedlings. *African Plant Protection*, *4*(2), 123–128. https://journals.co.za/doi/pdf/10.10520/AJA10233121_169

Kouadio, L., Jarroudi, M. E., Belabess, Z., Laasli, S., Roni, M. Z. K., Amine, I. D. I., Mokhtari, N., Mokrini, F., Junk, J., & Lahlali, R. (2023). A review on UAV-Based Applications for Plant Disease Detection and Monitoring. *Remote Sensing*, *15*(17), 4273. https://doi.org/10.3390/rs15174273

Kuswidiyanto, L. W., Noh, H., & Han, X. (2022). Plant disease diagnosis using deep learning based on aerial hyperspectral images: a review. *Remote Sensing*, *14*(23), 6031. https://doi.org/10.3390/rs14236031

Latif, M. A. (2019). Multi-crop recognition using UAV-based high-resolution NDVI time-series. *Journal of Unmanned Vehicle Systems*, *7*(3), 207–218. https://doi.org/10.1139/juvs-2018-0036

Li, M., Shamshiri, R. R., Weltzien, C., & Schirrmann, M. (2022). Crop monitoring using Sentinel-2 and UAV multispectral imagery: A comparison case study in northeastern Germany. *Remote Sensing*, *14*(17), 4426. https://doi.org/10.3390/rs14174426

Li, X., Lee, W. S., Li, M., Ehsani, R., Mishra, A. R., Yang, C., & Mangan, R. L. (2012). Spectral difference analysis and airborne imaging classification for citrus greening infected trees. *Computers and Electronics in Agriculture*, *83*, 32–46. https://doi.org/10.1016/j.compag.2012.01.010

Li, X., Lee, W. S., Li, M., Ehsani, R., Mishra, A. R., Yang, C., & Mangan, R. L. (2015). Feasibility study on Huanglongbing (citrus greening) detection based on WorldView-2 satellite imagery. *Biosystems Engineering*, *132*, 28–38. https://doi.org/10.1016/j.biosystemseng.2015.01.009

Maes, W. H., & Steppe, K. (2019). Perspectives for Remote Sensing with Unmanned Aerial Vehicles in Precision Agriculture. *Trends in Plant Science*, *24*(2), 152–164. https://doi.org/10.1016/j.tplants.2018.11.007

Mahlein, A. (2016). Plant disease detection by imaging sensors – parallels and specific demands for precision agriculture and plant phenotyping. *Plant Disease*, *100*(2), 241–251. https://doi.org/10.1094/pdis-03-15-0340-fe

Maimaitijiang, M., Sagan, V., Sidike, P., Daloye, A. M., Erkbol, H., & Fritschi, F. B. (2020). Crop monitoring using Satellite/UAV data fusion and machine learning. *Remote Sensing*, *12*(9), 1357. https://doi.org/10.3390/rs12091357

Maponya, P., & Mpandeli, S. (2012). Climate Change and Agricultural Production in South Africa: Impacts and Adaptation options. *Journal of Agricultural Science*, *4*(10). https://doi.org/10.5539/jas.v4n10p48

Maseko, B., & Coutinho, T. (2002). Pathogenicity of Phytophthora and Pythium species associated with citrus root rot in South Africa. *South African Journal of Botany*, *68*(3), 327–332. https://doi.org/10.1016/s0254-6299(15)30394-x

Meitz-Hopkins, J. C., Pretorius, M. C., Spies, C. F. J., Huisman, L., Botha, W. J., Langenhoven, S. D., & McLeod, A. (2013). Phytophthora species distribution in South African citrus production regions. *European Journal of Plant Pathology*, *138*(4), 733–749. https://doi.org/10.1007/s10658-013-0346-9

Mestas, A. (2018). *Environmental factors affecting phytophthora root rot of rhododendron* [Thesis, Oregon State University]. https://ir.library.oregonstate.edu/concern/graduate_thesis_or_dissertations/pg15bm51c

Mishra, P., Singh, U., Pandey, C., Mishra, P., & Pandey, G. (2019). Application of student's t-test, analysis of variance, and covariance. *Annals of Cardiac Anaesthesia/Annals of Cardiac Anaesthesia*, *22*(4), 407. https://doi.org/10.4103/aca.aca_94_19

Mishra, R. K. (2012). A review of Optical imagery and Airborne LiDAR data registration methods. *The Open Remote Sensing Journal*, *5*(1), 54–63. https://doi.org/10.2174/1875413901205010054

Moriya, É. a. S., Imai, N. N., Tommaselli, A. M. G., Berveglieri, A., Santos, G. H., Soares, M. A., Marino, M., & Reis, T. T. (2021). Detection and mapping of trees infected with citrus gummosis using UAV hyperspectral data. *Computers and Electronics in Agriculture*, *188*, 106298. https://doi.org/10.1016/j.compag.2021.106298

Musci, M. A., Persello, C., & Lingua, A. M. (2020). UAV images and deep-learning algorithms for detecting flavescence doree disease in grapevine orchards. *The International Archives of the Photogrammetry, Remote Sensing and Spatial Information Sciences*, *XLIII-B3-2020*, 1483–1489. https://doi.org/10.5194/isprs-archives-xliii-b3-2020-1483-2020

Nowakowski, A., Mrziglod, J., Spiller, D., Bonifacio, R., Ferrari, I., Mathieu, P. P., Garcia-Herranz, M., & Kim, D. (2021). Crop type mapping by using transfer learning. *International Journal of Applied Earth Observation and Geoinformation*, *98*, 102313. https://doi.org/10.1016/j.jag.2021.102313

Ollinger, S. V. (2010). Sources of variability in canopy reflectance and the convergent properties of plants. *New Phytologist*, *189*(2), 375–394. https://doi.org/10.1111/j.1469-8137.2010.03536.x

Osco, L. P., Marcato, J., Junior, Ramos, A. P. M., De Castro Jorge, L. A., Fatholahi, S. N., De Andrade Silva, J., Matsubara, E. T., Pistori, H., Gonçalves, W. N., & Li, J. (2021). A review on deep learning in UAV remote sensing. *International Journal of Applied Earth Observation and Geoinformation*, *102*, 102456. https://doi.org/10.1016/j.jag.2021.102456

Osco, L. P., Nogueira, K., Ramos, A. P. M., Pinheiro, M. M. F., Furuya, D. E. G., Gonçalves, W. N., De Castro Jorge, L. A., Marcato, J., Junior, & Santos, J. a. D. (2021). Semantic segmentation of citrus-orchard using deep neural networks and multispectral UAV-based imagery. *Precision Agriculture*, *22*(4), 1171–1188. https://doi.org/10.1007/s11119-020-09777-5

Pádua, L., Marques, P., Martins, L. M., Sousa, A. M. R., Peres, E., & Sousa, J. J. (2020). Monitoring of chestnut trees using machine learning techniques applied to UAV-Based multispectral data. *Remote Sensing*, *12*(18), 3032. https://doi.org/10.3390/rs12183032

Park, E., Kim, Y., Faqeerzada, M. A., Kim, M. S., Baek, I., & Cho, B. (2023). Hyperspectral reflectance imaging for nondestructive evaluation of root rot in Korean ginseng (Panax ginseng Meyer). *Frontiers in Plant Science*, *14*. https://doi.org/10.3389/fpls.2023.1109060

Peng, Y., Dallas, M. M., Ascencio-Ibáñez, J. T., Hoyer, J. S., Legg, J., Hanley-Bowdoin, L., Grieve, B., & Yin, H. (2022). Early detection of plant virus infection using multispectral imaging and spatial–spectral machine learning. *Scientific Reports*, *12*(1). https://doi.org/10.1038/s41598-022-06372-8

Phytophthora | Citrus diseases. (2013). https://idtools.org/citrus_diseases/index.cfm?packageID=2&entityID=180
Poláček, M., Arizpe, A., Hüther, P., Weidlich, L., Steindl, S., & Swarts, K. (2023). Automation of tree-ring detection and measurements using deep learning. *Methods in Ecology and Evolution*, *14*(9), 2233–2242. https://doi.org/10.1111/2041-210x.14183

Popescu, D., Ichim, L., & Stoican, F. (2023). Orchard monitoring based on unmanned aerial vehicles and image processing by artificial neural networks: a systematic review. *Frontiers in Plant Science*, *14*. https://doi.org/10.3389/fpls.2023.1237695

R, M. T., Kumar, V., V., Kumar, D., V., Geman, O., Margala, M., & Guduri, M. (2023). The stratified K-folds cross-validation and class-balancing methods with high-performance ensemble classifiers for breast cancer classification. *Healthcare Analytics*, *4*, 100247. https://doi.org/10.1016/j.health.2023.100247

Rai, N., & Flores, P. (2021). Leveraging transfer learning in ArcGIS Pro to detect doubles in a sunflower field. *American Society of Agricultural and Biological Engineers Annual International Virtual Meeting*, *3*, 1. https://doi.org/10.13031/aim.202100742

Ramírez-Gil, J. G., Castañeda-Sánchez, D. A., & Morales-Osorio, J. G. (2016). Production of avocado trees infected with Phytophthora cinnamomi under different management regimes. *Plant Pathology*, *66*(4), 623–632. https://doi.org/10.1111/ppa.12620

RedEdge-P Integration Guide. (2024, April 18). MicaSense Knowledge Base. https://support.micasense.com/hc/en-us/articles/4410824602903-RedEdge-P-Integration-Guide

Ristaino, J. B., Anderson, P. K., Bebber, D. P., Brauman, K. A., Cunniffe, N. J., Fedoroff, N. V., Finegold, C., Garrett, K. A., Gilligan, C. A., Jones, C. M., Martin, M. D., MacDonald, G. K., Neenan, P., Records, A., Schmale, D. G., Tateosian, L., & Wei, Q. (2021). The persistent threat of emerging plant disease pandemics to global food security. *Proceedings of the National Academy of Sciences of the United States of America*, *118*(23). https://doi.org/10.1073/pnas.2022239118

Salgadoe, A. S. A., Robson, A. J., Lamb, D. W., Dann, E. K., & Searle, C. (2018). Quantifying the severity of phytophthora root rot disease in avocado trees using image analysis. *Remote Sensing*, *10*(2), 226. https://doi.org/10.3390/rs10020226

Sangjan, W., McGee, R. J., & Sankaran, S. (2022). Optimization of UAV-Based imaging and image processing orthomosaic and point cloud approaches for estimating biomass in a forage crop. *Remote Sensing*, *14*(10), 2396. https://doi.org/10.3390/rs14102396

Sarkar, S. K., Das, J., Ehsani, R., & Kumar, V. (2016). Towards Autonomous Phytopathology: Outcomes and challenges of citrus greening disease detection through close-range remote sensing. *International Conference on Robotics and Automation*. https://doi.org/10.1109/icra.2016.7487719

Savita, G. S. V., & Nagpal, A. (2012). Citrus diseases caused by phytophthora species. *GERF Bulletin of Biosciences*, *3*(1), 18–27. https://www.academia.edu/5763877/Citrus_diseases_caused_by_Phytophthora_species

Shahi, T. B., Xu, C., Neupane, A., & Guo, W. (2023). Recent advances in crop disease detection using UAV and deep learning techniques. *Remote Sensing*, *15*(9), 2450. https://doi.org/10.3390/rs15092450

Swart, L. (2018). *Understanding citrus replant disease in South Africa with the aim of developing a methyl bromide free management strategy* [Thesis, Stellenbosch University]. https://scholar.sun.ac.za/handle/10019.1/103883

Taylor, L., & Nitschke, G. (2017). Improving deep learning using generic data augmentation. *arXiv (Cornell University)*, *Proceedings of the 2018 IEEE Symposium Series on Computational Intelligence*, 1542–1547. https://doi.org/10.48550/arxiv.1708.06020

Terven, J., Cordova-Esparza, D. M., Ramirez-Pedraza, A., & Chavez-Urbiola, E. A. (2023). Loss functions and metrics in deep learning. *arXiv (Cornell University)*. https://doi.org/10.48550/arxiv.2307.02694

Trajkovski, K. K., Grigillo, D., & Petrovič, D. (2020). Optimization of UAV flight missions in steep terrain. *Remote Sensing*, *12*(8), 1293. https://doi.org/10.3390/rs12081293

Wang, Y. E., Wei, G., & Brooks, D. (2019). Benchmarking TPU, GPU, and CPU platforms for deep learning. *arXiv (Cornell University)*. https://doi.org/10.48550/arxiv.1907.10701

Wiesman, Z. (2009). *Desert olive oil cultivation: Advanced Biotechnologies*. Academic Press. https://www.sciencedirect.com/book/9780123742575/desert-olive-oil-cultivation

Yue, J., Lei, T., Li, C., & Zhu, J. (2012). The application of unmanned aerial vehicle remote sensing in quickly monitoring crop pests. *Intelligent Automation and Soft Computing/Intelligent Automation & Soft Computing*, *18*(8), 1043–1052. https://doi.org/10.1080/10798587.2008.10643309

Zarco-Tejada, P., Hornero, A., Hernández-Clemente, R., & Beck, P. (2018). Understanding the temporal dimension of the red-edge spectral region for forest decline detection using high-resolution hyperspectral and Sentinel-2a imagery. *ISPRS Journal of Photogrammetry and Remote Sensing*, *137*, 134–148. https://doi.org/10.1016/j.isprsjprs.2018.01.017

Zentmyer, G. A. (1988). Origin and distribution of four species of phytophthora. *Transactions of the British Mycological Society*, *91*(3), 367–378. https://doi.org/10.1016/s0007-1536(88)80111-6

Zhou, X., Li, Y., Luo, Y., Sun, Y., Su, Y., Tan, C., & Liu, Y. (2022). Research on remote sensing classification of fruit trees based on Sentinel-2 multi-temporal imageries. *Scientific Reports*, *12*(1), 11549. https://doi.org/10.1038/s41598-022-15414-0